Measurement report: Formation and brownness of aqueous secondary organic aerosol from the aged biomass-burning emissions in the Sichuan Basin, China

1   Chao Peng[1,2,3,4], Yan Ding[4], Zhenliang Li[1,2,3], Tianyu Zhai[4], Xinping

2   Yang[4], Mi Tian[6], Yang Chen[5], Xin Long[5], Haohui Tang[6], Guangming

3   Shi[7], Liuyi Zhang[8], Kangyin Zhang[8], Fumo Yang[7], and Chongzhi Zhai[1,2,3]

4   [1]Chongqing Academy of Ecology and Environmental Sciences, Chongqing, 401336,

5   China

6   [2]Chongqing Branch Academy of Chinese Research Academy of Environmental

7   Sciences, Chongqing, 401336, China

8   [3]Chongqing Key Laboratory of Urban Atmospheric Environment Observation and

9   Pollution Prevention, Chongqing, 401336, China

10 [4]Chinese Research Academy of Environmental Sciences, Beijing 100012, China

11 [5]Chongqing Institute of Green and Intelligent Technology, Chinese Academy of

12 Sciences, Chongqing, 400714, China

13 [6]College of Environment and Ecology, Chongqing University, Chongqing, 400045,

14 China

15 [7]College of Carbon Neutrality Future Technology, Sichuan University, Chengdu,

16 610065, China

17 [8]Chongqing Three Gorges University, Wanzhou, 404000, China

18 **Correspondence:** Chao Peng (pengchao0623@sina.com) and Chongzhi Zhai

19 (czz66818@sina.com)

Abstract. Secondary organic aerosol (SOA), formed via complex chemical mechanisms, is a major contributor to atmospheric aerosol pollution and climate forcing worldwide. Aqueous-phase oxidation serves as an important pathway for SOA formation, with aqueous SOA (aqSOA) exhibiting light absorption across the ultraviolet–visible range. This study investigates the formation and absorption properties of aqSOA in the Sichuan Basin, China. Results indicate that aqSOA mainly originated from aged biomass-burning emissions through aqueous-phase processing rather than from gas-phase photochemical oxidation, particularly under high aerosol liquid water content conditions during pollution periods. Substantial enhancement of brown carbon absorption by SOA was observed between 370 and 660 nm (27.5%−43.2%). These findings highlight the significant contribution of aqSOA formation from aged biomass-burning emissions to the brown carbon budget and absorption, especially at night. The mean aerosol absorption Ångström exponents between 370 and 880 nm ($AAE_{370–880}$) were 1.95, which is higher than the values reported for fresh and photochemically aged biomass-burning emissions. This study elucidates the formation and light-absorbing characteristics of aqSOA derived from aged biomass-burning emissions and highlights the important role of aqueous-phase reactions in aerosol pollution and radiative absorption.

Keywords: Particulate matter; Secondary organic aerosol; Aqueous-phase oxidation; Aged biomass-burning emissions; Brown carbon

删除[Chao]: Here, we reported

删除[Chao]: reactions

删除[Chao]: photochemical reactions

删除[Chao]: ed

删除[Chao]: as

2

1 Introduction

Organic aerosol (OA) constitutes a dominant fraction (20−90%) of atmospheric aerosol, with significant implications for air quality and climate forcing (Jimenez et al., 2009). Field observations consistently indicate that secondary OA (SOA), formed by the atmospheric oxidation of volatile organic compounds (VOCs) and primary OA (POA), accounts for most OA worldwide (Ervens et al., 2011; Huang et al., 2014; Kourtchev et al., 2016). Recent results demonstrate that aqueous-phase oxidation serves as an important pathway for SOA formation, and aqueous SOA (aqSOA) exhibits light absorption across the ultraviolet−visible (UV−Vis) range (Gilardoni et al., 2016; Lim et al., 2010; McNeill 2015; Powelson et al., 2014; Sun et al., 2010). However, the formation mechanisms and absorption properties of aqSOA remain poorly understood, which hinders efforts to improve air quality and reduce uncertainties in global climate estimates.

Several studies suggest that aqSOA represents a major component of SOA formed in fog, clouds and aerosol water (Ervens et al., 2011; Ortiz-Montalvo et al., 2012; Tan et al., 2012; Xu et al., 2022). Oxygenated VOCs with high water solubility and low Henry's law constants, such as methylglyoxal and glycolaldehyde, are important aqSOA precursors (Ortiz-Montalvo et al., 2012; Tan et al., 2012). Limited laboratory studies have demonstrated that levoglucosan and phenolic species produced from biomass burning can also act as aqSOA precursors (Yu et al., 2016; Zhao et al., 2014). Gilardoni et al. (2016) reported direct ambient observations of aqSOA formation from biomass-burning emissions in fog, water and wet aerosol. Additionally, recent studies have reported that aqSOA with high molecular weight (e.g., 4-ethylphenol), formed through aqueous-phase photochemical oxidation, can exhibit strong light absorptivity in the UV range (Herrmann et al., 2015; Ye et al., 2019). Furthermore, previous laboratory studies have demonstrated that certain aqSOA components, such as π-conjugated compounds and imidazoles with C=N bonds, produced by aldol condensation and aqueous-phase carbonyl compound reactions, respectively, strongly absorb light in the near-UV region (Drozd and

删除[Chao]: also

删除[Chao]: n

删除[Chao]: would

3

69 McNeill, 2014; Kampf et al., 2012; Nozière and Esteve, 2007; Powelson et al., 2014).

70 Despite numerous studies on the formation and optical properties of aqSOA, limited

71 ambient observations still hinder a better understanding of its role in atmospheric

72 chemistry and climate.

73   China has experienced severe $PM_{2.5}$ pollution under stagnant high-humidity

74 conditions, during which SOA, a major $PM_{2.5}$ component, originated largely from

75 fossil fuel combustion and biomass burning (Huang et al., 2014; Wang et al., 2016;

76 Wang et al., 2021; Xu et al., 2022). Field observations indicate that highly oxidized

77 SOA can form through aqueous-phase processing driven by acid-catalyzed oxidation

78 (Meng et al., 2020; Xu et al., 2017), and aqSOA is derived from biomass-burning OA

79 (BBOA) and fossil-fuel OA through aqueous-phase reactions (Wang et al., 2021; Zhao

80 et al., 2019). Limited laboratory studies have reported that aqueous-phase reactions

81 serve as an important oxidation pathway for nitrophenol products such as

82 5-nitrovanillin and 4-nitroguaiacol, which exhibit strong UV absorption and higher

83 formation and transformation rates in more acidic solutions (Kroflic et al., 2015; Li et

84 al., 2023; Pang et al., 2019; Yang et al., 2021). However, observations of aqSOA

85 formation and optical properties in China remain limited, with most research focusing

86 on the North China Plain (NCP). Similar to the NCP, the Sichuan Basin (SCB),

87 characterized by high humidity and frequent biomass burning, is also the main region

88 with severe aerosol pollution in China (Tian et al., 2019; Wang et al., 2018; Yang et

89 al., 2011).

90   Previous research has reported that aqSOA from different regions can exhibit

91 distinct formation mechanisms and optical properties due to varying emission sources

92 and ambient conditions (Bao et al., 2023; Bao et al., 2024; Wang et al., 2021; Xu et al.,

93 2017). Wang et al. (2021) reported the rapid aqueous-phase conversion of fossil-fuel

94 primary OA (FF-POA) to aqSOA under high-humidity conditions during a winter

95 haze event in Beijing, China, with the resulting aqSOA exhibiting substantially lower

96 light absorption than its primary precursor due to decreased aromaticity. Similarly,

97 Huang et al. (2023) demonstrated that the aqueous-phase oxidation of fossil fuel

98 combustion emissions played a critical role in SOA formation under high relative

删除[Chao]: s

删除[Chao]: with

99   humidity (RH) conditions during winter. Xu et al. (2022) reported that biomass

100   burning is a significant non-fossil source of aqSOA under high RH and high aerosol

101   liquid water content (ALWC), especially during the fall-to-winter period, when open

102   burning of post-harvest agricultural crop residues is widespread in China. While

103   aqSOA formation has been extensively studied during winter, autumn—despite

104   featuring both high ALWC and strong biomass-burning emissions—has received

105   considerably less attention (Feng et al., 2022; Qiu et al., 2016; Zhao et al., 2019). In

106   contrast to these studies in the NCP, research in the SCB has reported that the effect of

107   aqueous-phase reactions on oxygenated OA (OOA) formation was significant when

108   ALWC was below 200 $\mu g\ m^{-3}$, but became insignificant when ALWC exceeded 200

109      $\mu g\ m^{-3}$. Additionally, aqueous-phase oxidation probably did not contribute to the

110   decay of brown carbon (BrC) during summer in the SCB (Bao et al., 2024). In the

111   SCB, autumn is the typical biomass-burning season following the harvest of rape and

112   rice, during which biomass burning contributes significantly more to OA than in other

113   seasons (Chen et al., 2017; Tao et al., 2014; Yang et al., 2019). In summary, the

114   intensive biomass-burning emissions and high ALWC during autumn in the SCB

115   likely result in aqSOA formation pathways that differ from those in other seasons. To

116   date, limited studies have explored the dynamic evolution and optical properties of

117   aqSOA in the SCB, especially during autumn, leaving ambient aqSOA processing

118   poorly understood. Therefore, a more detailed characterization of the aqSOA

119   formation and optical properties is important to reveal the key factors contributing to

120   haze formation in this region.

121   In this study, a time-of-flight aerosol chemical speciation monitor (ToF-ACSM)

122   and a series of collocated instruments were deployed to characterize the dynamic

123   evolution of aqSOA from biomass burning under real ambient conditions. The study

124   was conducted in a typical city with relatively severe air pollution in the SCB from

125   October 21 to November 23, 2022. Observations revealed that haze formation was

126   significantly driven by BBOA and aqSOA. This study demonstrates that aqSOA forms

127   from aged BBOA through aqueous-phase reactions. Furthermore, the results

128   demonstrate that aqSOA derived from aged BBOA exhibits strong UV absorption and

129 contributes to positive radiative forcing. These results elucidate the formation and
130 light-absorbing properties of aqSOA from aged biomass-burning emissions, providing
131 insights for improved simulations of its atmospheric and climatic impacts.

132 **2 Methods**

133 **2.1 Sampling site**

134 An intensive field campaign investigating the chemical and physical properties
135 of aerosols was conducted at a site in Yongchuan, China, (29°21′25″ N, 105°54′6″ E),
136 a city experiencing severe aerosol pollution, from October 21 to November 23, 2022.
137 This site is representative of an urban environment, surrounded by restaurants,
138 shopping malls, and residential buildings, and is located in a parallel ridge-and-valley
139 area between the two megacities of the SCB (Chongqing center and Chengdu) (Fig.
140 S1). It is primarily influenced by multiple local emission sources, including traffic
141 (arterial roads 600 m to the east and 300 m to the west) and a variety of residential
142 activities such as biomass burning and fossil fuel combustion. The absence of
143 dynamic interference from neighbouring buildings allowed the measurements to
144 clearly capture the characteristics and evolution of haze pollution at this site.

145 **2.2 Instrumentation**

146 During the campaign, non-refractory aerosol (NR-PM$_{2.5}$) species, including OA,
147 ammonium (NH$_4$), nitrates (NO$_3$), sulfates (SO$_4$), and chlorides (Chl), were measured
148 online using the ToF-ACSM (Aerodyne Research Inc.). Ambient aerosols were
149 pumped into the ToF-ACSM at a flow rate of 3 L min^{-1} through a PM$_{2.5}$ cyclone
150 (URG-2000-30ED) and a Nafion dryer (MD-110-48S, Perma Pure, Inc.), reducing the
151 RH to below 30%. The measurement principle has been described in detail in
152 previous studies (Fröhlich et al., 2013; Ng et al., 2011c).

删除[Chao]: the

153 Aerosol light absorption (Abs$_\lambda$) and equivalent black carbon (BC$_\lambda$) mass
154 concentrations were measured in real time at seven wavelengths (370, 470, 520, 590,
155 660, 880, and 950 nm) using an aethalometer (AE33, Magee Scientific). Sampled

particles were dried using a Nafion dryer (MD-70024S-3, Perma Pure, Inc.) before measurements. The light attenuation coefficients were converted to Abs_λ using the real-time compensation parameter, and the nonlinear loading effects of quartz filters were corrected online through parallel measurements of attenuation values (ATN1 and ATN2) (Coen et al., 2010; Drinovec et al., 2015). The scattering effects of quartz filters were modified automatically by a fixed multiple-scattering parameter (2.14) (SI Text S3). Detailed measurement methods and principles of AE33 are described in Drinovec et al. (2015).

During the campaign, gaseous species (including O_3, NO_2, and CO) were continuously measured by gas analyzers (49i, 42i, and 48i, Thermo Scientific) that were maintained and calibrated weekly. Hourly meteorological parameter data, including temperature (T), RH, and $PM_{2.5}$ mass concentrations, were obtained from the National Environmental Monitoring Station, located near our sampling site (http://www.cnemc.cn/, last access: 30 November 2022).

2.3 Data analysis

2.3.1 ToF-ACSM data analysis

The raw mass spectra data measured by the ToF-ACSM were analyzed using Tofware v2.5.13 (Tofwerk AG) in Igor Pro 6.37 (WaveMetrics, Inc.). The ionization efficiency and relative ionization efficiency (RIE) were regularly calibrated using a scanning mobility particle sizer, consisting of a differential mobility analyzer (SMPS 3081A, TSI) and a condensation particle counter (CPC 3775, TSI). A comprehensive overview of the operation and calibration procedures of the ToF-ACSM is provided in Bao et al. (2023). In accordance with previous studies, the default RIE values for OA, NO_3, and Chl were set to 1.4, 1.1, and 1.3, respectively (Canagaratna et al., 2007; Elser et al., 2016). The ionization efficiency value (236 ions pg^{-1}) and RIE values of SO_4 (1.2) and NH_4 (4.3) were estimated from the calibrations of pure ammonium sulfate and ammonium nitrate (ANMF), respectively. Meanwhile, a particle collection efficiency (CE) was introduced to compensate for the particle losses associated with

7

the particle bounce at the vaporizer, which is affected by aerosol acidity, the contribution of ammonium nitrate, and phase state (Matthew et al., 2008). Middlebrook et al. (2012) developed a CE algorithm for the ToF-ACSM to quantify aerosol species. Their results indicated that a constant CE value of 0.45 should be used when: (1) ANMF is below 40% or (2) particles are either partially or fully neutralized. In this study, aerosol particles were dried using a Nafion dryer (RH < 30%) before sampling by the ToF-ACSM, and ANMF was consistently maintained below 40%. As shown in Fig. S2, the average ratio of the measured NH_4 to the predicted NH_4, which is required to fully neutralize SO_4, NO_3, and Chl, was approximately 1. Under these conditions, the CE value typically used at this site was not affected. The typical default CE value (0.5) was applied throughout the sampling period, which was consistent with previous research (Bao et al., 2025; Peng et al., 2025; Sun et al., 2016a; Sun et al., 2016b; Zhao et al., 2019). While the typical default CE is 10% higher than 0.45, the difference is small, considering the 30% uncertainty determined for CE (Bahreini et al., 2009). Additionally, the strong correlation between $NR\text{-}PM_{2.5}$ and $PM_{2.5}$ mass concentrations supports the validity of the CE value (Fig. S3).

The mass spectral matrix of OA for m/z 10−120 was analysed through positive matrix factorization (PMF) with the multilinear engine (ME-2) implemented in SoFi (Source Finder, version 6.3) (Canonaco et al., 2013; Paatero 1999; Paatero and Tapper 1994). Briefly, an unconstrained PMF analysis was performed to determine the number and types of source factors. Subsequently, the constrained ME-2 approach was applied to minimize rotational ambiguity by testing a-values from 0 to 1 in steps of 0.1 (Elser et al., 2016; Wang et al., 2019b; Zhong et al., 2021). Ions with a signal-to-noise ratio (SNR) below 0.2 were discarded, whereas those with an SNR between 0.2 and 2 were downweighted by a factor of 2 (Bao et al., 2023; Paatero and Hopke 2003). Finally, five OA factors were resolved with the rotational parameter set to zero ($f_{peak} = 0$), including three POA factors (BBOA, coal-combustion OA (CCOA), and hydrocarbon-like OA (HOA)) and two SOA factors (OOA and aqSOA) (Fig. S9 and S10). Detailed diagnostic plots of the PMF results are presented in the Supporting

214 Information (Fig. S4−S10), and the details of OA source apportionment procedures
215 are described in SI Text S1.

2.3.2 Aerosol liquid water content

217 ALWC is controlled by meteorological conditions (T and RH) as well as by
218 inorganic and OA components. During the campaign, ALWC controlled by the
219 inorganic fraction was estimated with the ISORROPIA-II thermodynamic model,
220 based on mass concentrations of ammonium, nitrate, sulfate, and chloride measured
221 by the ToF-ACSM, together with the meteorological parameters (T and RH) from the
222 National Environmental Monitoring Station (Fountoukis and Nenes, 2007). The
223 calculations were performed in forward type and metastable mode within
224 ISORROPIA-II (Hennigan et al., 2015). The model simulated the thermodynamic
225 equilibrium of the $NH_4^+-SO_4^{2-}-NO_3^--Cl^--H_2O$ system and subsequently calculated
226 the ALWC. Following established methods, the organic contribution to ALWC was
227 estimated using the Zdanovskii−Stokes−Robinson mixing rule, as discussed in SI Text
228 S2 (Guo et al., 2015; Huang et al., 2020; Nguyen et al., 2016; Xu et al., 2022). In
229 this study, the ALWC with organic species ranged from 0.1 to 35.2 µg m^{-3}, with an
230 average of 1.9 ± 3.0 µg m^{-3}, accounting for 3.7 ± 2.2% of total ALWC. As organic
231 species had minor effects on total ALWC (< 5%), the ALWC was determined only
232 considering inorganic species (Chen et al., 2021; Guo et al., 2015; Liu et al., 2017).

2.3.3 Light absorption measurements

234 The Abs_λ was partitioned into contributions from BC and BrC, a group of
235 colored OA compounds, denoted as $Abs_{\lambda,BC}$ and $Abs_{\lambda,BrC}$, respectively, such that
236 $Abs_\lambda = Abs_{\lambda,BC} + Abs_{\lambda,BrC}$, and characterized by the absorption Ångström exponent
237 (AAE) (Laskin et al., 2015). Here, Abs_λ was derived from BC_λ mass concentrations at
238 each wavelength using the mass absorption cross-section (MAC_λ)
239 ($Abs_\lambda = BC_\lambda \times MAC_\lambda$), with MAC_λ values assumed to be 18.47, 14.54, 13.14, 11.58,
240 10.35, 7.77, and 7.19 m^2 g^{-1} at 370, 470, 520, 590, 660, 880, and 950 nm, respectively

241 (Drinovec et al., 2015; Zhu et al., 2017). Absorbance at 880 nm (Abs_{880}) was

242 attributed solely to BC. The following formula was used to determine $Abs_{\lambda,BC}$ values

243 (Drinovec et al., 2015; Kirchstetter and Novakov, 2004; Moosmüller et al., 2009; Qin

244 et al., 2018; Wang et al., 2021; Zhu et al., 2017):

$$Abs_{\lambda,BC} = Abs_{880} \times (880/\lambda)^{-AAE_{BC}} \qquad (1)$$

$$AAE_{BC} = -\log_{10}(Abs_{880}/Abs_{950}) \div \log_{10}(880/950) \qquad (2)$$

247 A detailed description of $Abs_{\lambda,BC}$ and $Abs_{\lambda,BrC}$ calculations is provided in SI Text

248 S3. Previous studies have demonstrated that AAE_{BC} is sensitive to the refractive index,

249 size distribution, and coating state of carbonaceous aerosols (Gyawali et al., 2009;

250 Lack and Langridge, 2013; Li et al., 2019). In this study, the uncertainties in Abs_{BC}

251 and Abs_{BrC} estimations were analyzed (Text S3). The relative uncertainties of Abs_{BC}

252 and Abs_{BrC} were [−46%, +21%] and [−112%, +42%] at 370 nm, respectively. $Abs_{\lambda,BrC}$

253 comprises contributions from primary and secondary BrC ($Abs_{\lambda,BrC,pri}$ and $Abs_{\lambda,BrC,sec}$).

254 $Abs_{\lambda,BrC,sec}$ was calculated using the minimum R-squared method (MRS) at each

255 wavelength (Wang et al., 2019b; Wu and Yu, 2016; Wu et al., 2024). Further details

256 on the MRS method and $Abs_{\lambda,BrC,sec}$ estimation are provided in SI Text S3.

257 The light absorption contribution of each OA component at each wavelength, as

258 analyzed using multiple linear regression (Qin et al., 2018; Xie et al., 2019), is

259 expressed as follows:

260 $Abs_{BrC} = a \times [OOA] + b \times [BBOA] + c \times [CCOA] + d \times [aqSOA] + e \times [HOA]$ (3)

261 where [OOA], [BBOA], [CCOA], [aqSOA], and [HOA] denote the mass

262 concentrations of the corresponding OA components. Coefficients a–e are constants

263 used to optimize the Abs_{λ} of each OA component and are equivalent to MAC values

264 at each wavelength (i.e., a–e at 370 nm represented $MAC_{370,OOA}$, $MAC_{370,BBOA}$,

265 $MAC_{370,CCOA}$, $MAC_{370,aqSOA}$, and $MAC_{370,HOA}$, respectively). Here, the normalized

266 mean bias, root mean square error, and index of agreement were used to evaluate the

267 performance of the multiple linear regression method (SI Text S4) (Li et al., 2011).

268 The index of agreement values for $Abs_{370,BrC}$ and $Abs_{470,BrC}$ were 0.99 and 1.00,

269 respectively, both exceeding 0.95. The slopes of the linear regression between the

270 AE33-measured and MLR-estimated absorption coefficients were 0.81 and 0.96 for

271 $Abs_{370,BrC}$ and $Abs_{470,BrC}$ (close to unity), respectively. These results indicate good

272 agreement between the AE33 measurement and the MLR-reconstructed $Abs_{370,BrC}$.

3 Results and discussion

3.1 Enhanced OA formation from BBOA and aqSOA during pollution periods

275 The temporal variations of $PM_{2.5}$ species concentrations, meteorological

276 parameters, $Abs_{370,BrC}$ and $MAC_{370,BrC}$ during the campaign are shown in Fig. 1. Wind

277 speeds were consistently low (0.3 ± 0.2 m s^{-1}), indicating stagnant atmospheric

278 conditions throughout the study period. The average concentrations of O_3 and NO_2

279 during the campaign were 24.8 ± 16.1 ppb and 14.2 ± 6.8 ppb, respectively. The total

280 $PM_{2.5}$ (BC + NR-$PM_{2.5}$) mass concentrations ranged from 7.0 to 175.5 µg m^{-3}, with an

281 average of 48.4 ± 27.8 µg m^{-3}. The average concentrations of OA, NO_3, SO_4, NH_4,

282 Chl, and BC were 24.1 ± 18.1, 8.3 ± 6.2, 6.2 ± 3.4, 5.2 ± 2.7, 0.2 ± 0.1, and 4.7 ± 2.9

283 µg m^{-3}, accounting for $46.6 \pm 10.7\%$, $17.7 \pm 8.0\%$, $13.2 \pm 4.4\%$, $11.2 \pm 2.7\%$, $0.3 \pm$

284 0.2%, and $10.1 \pm 5.5\%$ of total $PM_{2.5}$, respectively. OA accounted for the largest

285 fraction of $PM_{2.5}$, highlighting its significant contribution to $PM_{2.5}$ pollution in the

286 SCB (Bao et al., 2023; Wang et al., 2018). The OA fractions of $PM_{2.5}$ in this study are

287 comparable to those reported in wintertime studies in the SCB and are significantly

288 higher than those observed in winter in other Chinese regions (Table S1). Meanwhile,

289 elevated levels of $Abs_{370,BrC}$ and $MAC_{370,BrC}$, ranging from 5.8 to 210.2 Mm^{-1} ($42.4 \pm$

290 28.5 Mm^{-1}) and from 0.6 to 7.0 m^2 g^{-1} (2.1 ± 0.9 m^2 g^{-1}), respectively, were observed

291 during the campaign.

292 According to the Chinese National Ambient Air Quality Standard (GB

293 3095-2012) (MEP, 2012), the Grade I and Grade II 24-hour limits for $PM_{2.5}$ are 35 µg

294 m^{-3} and 75 µg m^{-3}, respectively. The Grade II limit, based on the WHO Phase-1

295 interim target (IT-1), is higher than the WHO Air Quality Guideline value (15 µg m^{-3}),

296 the EU daily limit (25 µg m^{-3}), and the U.S. 24-hour standard (35 µg m^{-3}). During the

297 campaign, the mean $PM_{2.5}$ concentration was 1.4 times the Grade I limit (35 µg m^{-3}).

298   Pollution periods (PP) were defined as days with daily $PM_{2.5}$ mass concentrations

299   exceeding the Grade II limit (75 μg m^{-3}), whereas days with $PM_{2.5}$ below 75 μg m^{-3}

300   were defined as clean periods (CP). During PP, the average mass concentrations of

301   BC + NR-$PM_{2.5}$ and OA were 2.5 and 3.1 times those during CP, respectively,

302   corresponding to 102.3 ± 26.9 and 57.4 ± 22.5 μg m^{-3}. As shown in Fig. 2, the

303   chemical composition of $PM_{2.5}$ differed substantially between PP and CP. Compared

304   with other species, a significantly higher contribution of OA was observed during PP

305   (56.6%) than during CP (46.6%) (Student's t-test, $p < 0.001$) (Fig. 2).

306   In this study, five OA factors were resolved using the PMF model. More details

307   are provided in SI Text S1, and the mass spectra of these factors are shown in Fig. S9.

308   HOA was characterized by alkyl fragment ion series at $C_nH^+_{2n-1}$ and $C_nH^+_{2n+1}$ (m/z 41,

309   43, 55, and 57), which are typical of primary combustion emissions (Elser et al., 2016;

310   Lanz et al., 2007). BBOA was identified by prominent signals at m/z 60 (mainly

311    $C_2H_4O_2^+$) and m/z 73 (mainly $C_3H_5O_2^+$), which correspond to fragments of

312   levoglucosan and mannosan from incomplete biomass burning (Alfarra et al., 2007).

313   CCOA showed high signals of unsaturated hydrocarbon ion fragments such as

314   PAH-related ion fragments (m/z 77, 91, 115), indicative of traditional coal combustion

315   (Sun et al., 2016a). OOA was distinguished by a dominant signal at m/z 44 (mainly

316   CO_2^+) and a strong correlation with oxygenated ions (Ng et al., 2011b). AqSOA also   删除[Chao]: a

317   correlated strongly with oxygenated ions, such as m/z 43 (mainly $C_2H_3O^+$) and m/z 44,

318   and exhibited a notably higher signal at m/z 29 (mainly CHO^+) than other OA factors,

319   consistent with previous reports (Sun et al., 2016a; Xu et al., 2019; Zhao et al., 2019;

320   Zhong et al., 2021). Moreover, BBOA correlated strongly with m/z 60 (mainly

321    $C_2H_4O_2^+$) and m/z 73 (Pearson's r^2 (r^2) = 0.85, 0.80, $p < 0.001$); CCOA was strongly

322   correlated with Chl and m/z 115 ($r^2 = 0.56$, 0.48, $p < 0.001$); HOA correlated with   删除[Chao]: was

323   NO_2 and m/z 41 ($r^2 = 0.47$, 0.59, $p < 0.001$); and OOA and aqSOA were significantly

324   correlated with NO_3/NH_4 ($r^2 = 0.77$, 0.75, $p < 0.001$) and SO_4/ALWC ($r^2 = 0.67$, 0.85,

325    $p < 0.001$), respectively (Fig. S10). These results confirm the robustness and

326   physicochemical plausibility of the five OA factors identified in this study. Overall,

327   the average concentration of BBOA was 8.6 ± 7.7 μg m^{-3} and accounted for the

328　highest proportion of OA (34.8 ± 11.2%), followed by OOA (5.5 ± 3.5 µg m^{-3}, 21.7 ±

329　11.4%), CCOA (4.0 ± 3.3 µg m^{-3}, 15.7 ± 7.1%), HOA (3.5 ± 2.8 µg m^{-3}, 14.6 ± 8.1%),

330　and aqSOA (3.3 ± 2.9 µg m^{-3}, 13.2 ± 5.9%) (Fig. 1). These results identified BBOA as

331　the dominant component of OA in autumn in the SCB. Notably, the fraction of BBOA

332　in OA in this study was much higher than those reported in wintertime studies in

333　China (Table S1).

334　　　The contributions of BBOA and aqSOA to OA increased from CP (31.7% and

335　12.6%, respectively) to PP (38.6% and 14.1%, respectively), whereas those of CCOA,

336　HOA, and OOA decreased. Significantly higher RH and ALWC were observed during

337　PP (58.5 ± 12.4% and 69.4 ± 30.3 µg m^{-3}, respectively) than during CP (49.8 ± 8.9%

338　and 37.1 ± 20.8 µg m^{-3}, respectively) ($p < 0.001$), whereas temperature showed no

339　significant difference ($p > 0.1$). The average wind speed during CP was 1.3 times that

340　during PP, reaching 0.32 ± 0.18 m s^{-1}. These results indicate that the atmosphere

341　during PP was characterized by stagnation, higher RH, and elevated ALWC, likely

342　leading to distinct sources and chemical processing of OA compared with CP.

343　　　Compared with CP, OA concentration exhibited an evident diurnal variation

344　during PP. As shown in Fig. 2, the OA concentration peaked at 12:00 local time (LT)

345　(82.7 µg m^{-3}) during daytime in PP, whereas in CP, the peak occurred at 21:00 LT.

346　During PP, OA increased rapidly at a rate of 7.8 µg m^{-3} hr^{-1} from 09:00 to 12:00 LT,

347　accompanied by a significant decrease in NO3. BBOA and aqSOA concentrations

348　exhibited similar diurnal patterns to OA, with high values during daytime and a rapid

349　increase from 09:00 to 12:00 LT during PP. Previous studies have indicated that the

350　aqSOA mass spectrum showed a higher signal at m/z 29 (CHO^{+}) than other OA

351　factors (Gilardoni et al., 2016; Meng et al., 2020; Wang et al., 2021). During PP, the

352　tracer ion fragments for BBOA (m/z 60) and aqSOA (m/z 29) peaked at 12:00 LT (1.2

353　µg m^{-3}) and 13:00 LT (4.3 µg m^{-3}), respectively. Additionally, ALWC correlated more

354　strongly with aqSOA concentration ($r^2 = 0.86$, $p < 0.001$) than with BBOA

355　concentration ($r^2 = 0.58$, $p < 0.001$). Both ALWC and aqSOA concentrations peaked

356　at 13:00 LT, later than the BBOA peak (12:00 LT), supporting that ALWC might play

357　a significant role in the chemical processing that converts BBOA to aqSOA during PP.

13

删除[Chao]: demonstrated

358   In contrast, odd oxygen ($O_x = O_3 + NO_2$) showed weak correlations with both OOA

359   and aqSOA concentrations throughout the campaign ($p > 0.1$, data not shown).

360   Although the average O_x concentration was higher during PP (51.1 ± 19.6 ppb) than

361   during CP (36.9 ± 14.0 ppb), no significant correlation was observed in either period.

362   These results suggest that gas-phase photochemical oxidation, might played a limited

363   role in SOA formation in this study.

364   In summary, these results suggest that OA was the dominant component of $PM_{2.5}$,

365   especially during PP in the SCB. During PP, BBOA and aqSOA contributed

366   significantly to the daytime increase in OA concentration. Previous studies have

367   shown that the autumn harvest period—specifically October and November—is

368   characterized by intensified biomass burning in the SCB, primarily due to

369   post-harvest crop-residue burning (Chen et al., 2017; Tao et al., 2014). Thus, daytime

370   aqSOA formation during PP might be related to high aerosol water content and BBOA

371   emissions (Bao et al., 2023; Chen et al., 2017; Chen et al., 2019; Tao et al., 2014).

372   Additionally, Gilardoni et al. (2016) found that aqSOA, such as guaiacol dimer

373   ($C_{14}H_{14}O_4^+$), could be formed from aged biomass-burning emissions in both fog water

374   and wet aerosol, especially under high ALWC conditions. To further explore the

375   formation of aqSOA from biomass-burning emissions through aqueous-phase

376   reactions, the next section discusses the dynamic evolution of aqSOA in relation to

377   BBOA.

删除[Chao]: photochemical reactions

删除[Chao]: ing

378
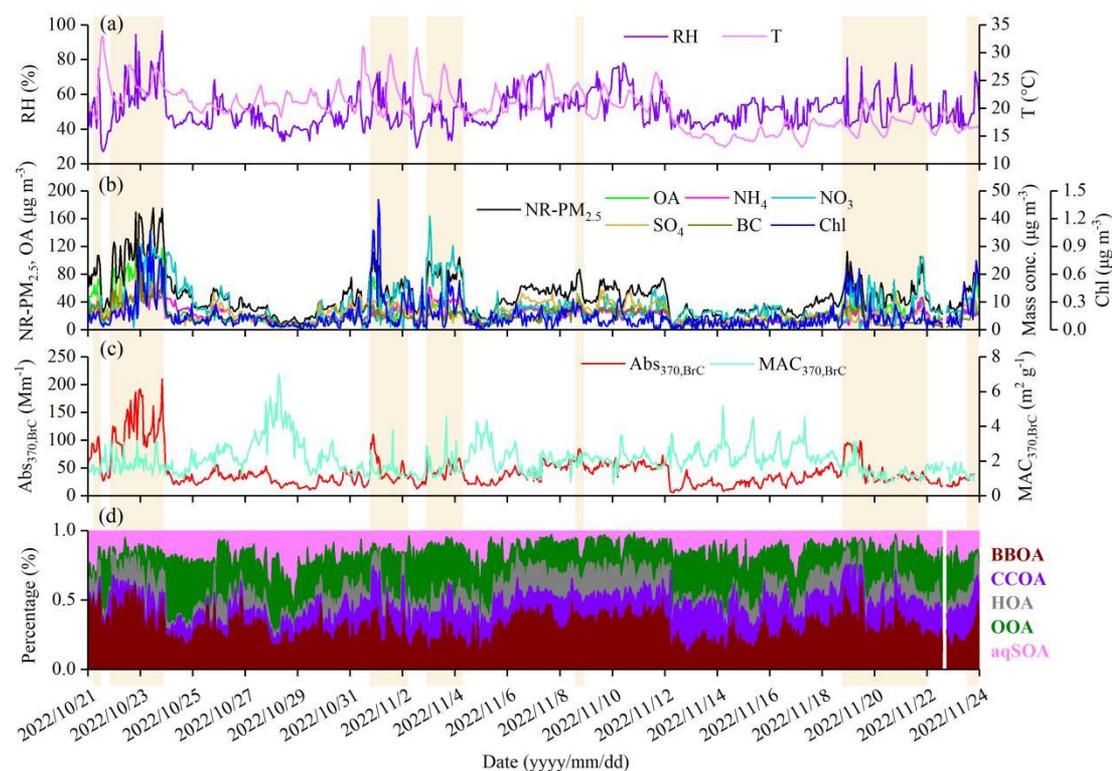
Figure 1. Time series of **(a)** RH and T, **(b)** NR-PM$_{2.5}$ species measured by the ToF-ACSM and BC,

(c) Abs$_{370,BrC}$ and MAC$_{370,BrC}$, and **(d)** mass fractions of OA factors during the campaign. The

pollution period (BC + NR-PM$_{2.5}$ > 75 µg m^{-3}) is highlighted by the shaded areas.

382
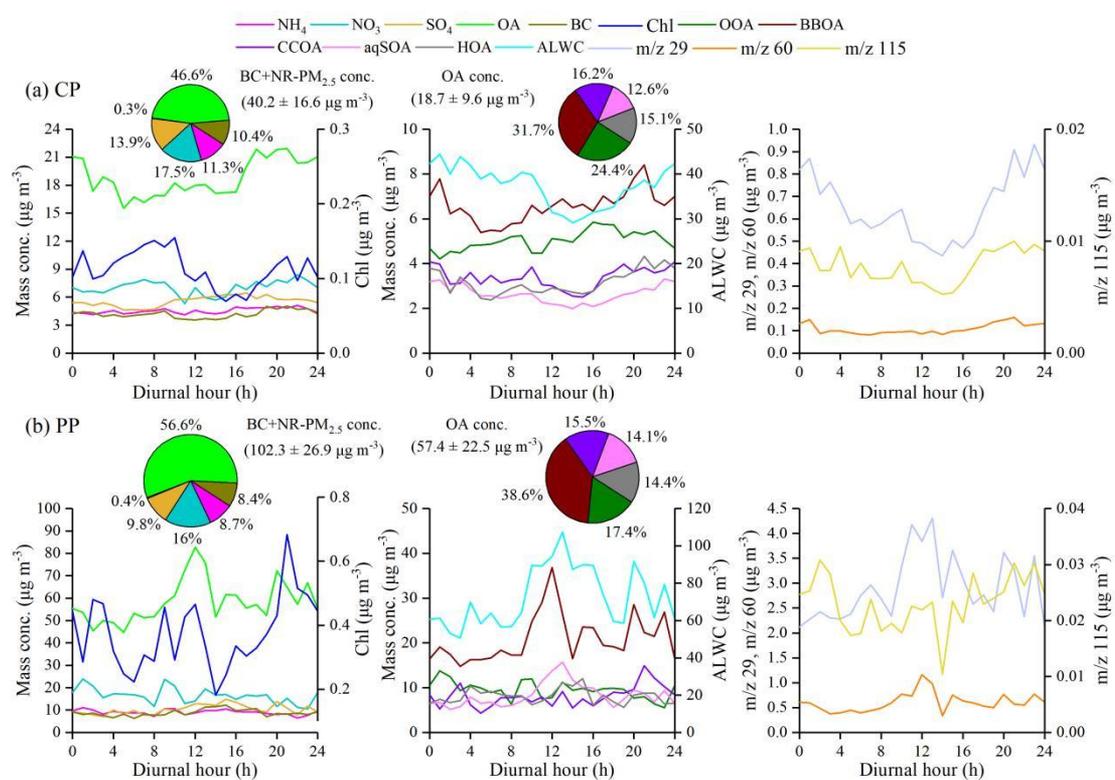
Figure 2. Diurnal variations of PM$_{2.5}$ species, BC, OA factors, m/z 29, m/z 60, and m/z 115 mass

concentrations during the **(a)** clean period (CP) (BC + NR-PM$_{2.5}$ < 75 μg m^{-3}) and **(b)** pollution

period (PP) (BC + NR-PM$_{2.5}$ > 75 μg m^{-3}). The pie charts on the left side of panels **(a)** and **(b)**

show the average mass contributions of different chemical compositions to BC + NR-PM$_{2.5}$ during

CP and PP, respectively. Meanwhile, the average mass contributions of OOA, BBOA, CCOA,

aqSOA, and HOA to OA are shown in the pie charts in the middle of panels **(a)** and **(b)**,

respectively.

3.2 Biomass-burning emissions as precursors for aqSOA

Figure 3 shows a strong positive correlation between the mass fraction (%) of

aqSOA in total PM$_{2.5}$ and ALWC during the campaign (r^2 = 0.64, p < 0.001). The

contribution of aqSOA increased with increasing f_{29} values (the normalized signal at

m/z 29). Notably, the aqSOA factor showed significantly higher f_{29} and f_{60} values

(0.167 and 0.011, respectively) than the OOA factor (0.017 and 0.002, respectively)

(Fig. S9). Moreover, both aqSOA concentrations and f_{29} were strongly correlated with

ALWC (r^2 = 0.85, 0.73, p < 0.001) (Fig. 3). The average oxygen-to-carbon ratio (O:C)

of the aqSOA factor (0.85) was 2.7 times that of the BBOA factor (0.31), whereas the

hydrogen-to-carbon (H:C) ratios were similar (1.74 for aqSOA and 1.81 for BBOA),

indicating the replacement of a hydrogen atom by an OH moiety (Lim et al., 2010; Ng

et al., 2011a). These results were similar to aqSOA results in Italy and Beijing

(Gilardoni et al., 2016; Zhao et al., 2019).

Previous studies indicate that aqueous-phase processes contribute to SOA

formation from fossil fuel emissions (Ervens et al., 2011; Huang et al., 2023; Wang et

al., 2021; Xu et al., 2022; Yan et al., 2017). Wang et al. (2021) and Xu et al. (2022)

have highlighted the role of aqueous-phase reactions in SOA formation, particularly in

regions with substantial anthropogenic emissions. In this study, a strong

anticorrelation was observed between the mass fraction of fossil-fuel-related OA

components (sum of CCOA, HOA and OOA) and ALWC at high f_{29} values (r^2 = 0.48,

p < 0.001, data not shown), consistent with recent findings (Wang et al., 2021). This

indicates that aqSOA may also be produced by aqueous-phase reactions of

删除[Chao]: ratio

412   fossil-fuel-related OA components.

413   Figure 4 shows the relationships between ALWC and the concentrations of OA

414   factors as well as f_{29} during the campaign. The mass concentrations of all five

415   resolved OA factors increased with increasing ALWC. However, compared with other

416   OA factors, aqSOA and BBOA increased more significantly, from 1.1 and 4.9 µg m^{-3}

417   to 5.2 and 10.8 µg m^{-3}, respectively, when 20 µg m^{-3} < ALWC < 60 µg m^{-3}. Notably,

418   only the aqSOA concentration continued to rise under high ALWC conditions (> 100

419   µg m^{-3}). This enhancement likely resulted from the formation of more water-soluble

420   organic species, such as glyoxal and methylglyoxal, which were subsequently

421   oxidized to aqSOA via aqueous-phase reactions in aerosol liquid water (Carlton et al.,

422   2007; Ervens et al., 2011; Tan et al., 2012).

423   As shown in Fig. 4b, the mass fraction of aqSOA increased significantly from

424   5% at ALWC < 20 µg m^{-3} to 17−22% at ALWC > 60 µg m^{-3}, accompanied by a

425   corresponding decrease in the OOA fraction. In contrast, the contributions of POA

426   (BBOA + CCOA + HOA) and SOA (OOA + aqSOA) remained relatively stable

427   across different ALWC levels (58−68% and 32−42% for POA and SOA, respectively).

428   This result suggests aqSOA forms more intensively than OOA through aqueous-phase

429   reactions, although it may also be formed from OOA, consistent with recent studies in

430   northwestern China (Zhao et al., 2019; Zhong et al., 2021).

431   Furthermore, f_{29} (CHO$^+$) increased from 0.010 to 0.227 as a function of ALWC

432   (Fig. 4b). A pronounced rise in f_{29} from 0.055 to 0.210 occurred when ALWC

433   increased from 60 µg m^{-3} to 100 µg m^{-3} ($p < 0.001$), tracking the concurrent increase

434   in OA mass concentrations (13.2−109.1 µg m^{-3}). Previous laboratory analyses of

435   organic standards have found that species without alcohol groups showed low f_{29} (<

436   0.05), while polyols and species with non-acid OH groups, which are common

437   products of biomass-burning emissions, displayed high f_{29} values (0.05–0.15)

438   (Canagaratna et al., 2015; Gilardoni et al., 2016; Zhao et al., 2014). This further

439   supports the potential formation of organic compounds with hydroxyl groups, such as

440   glyoxal and methylglyoxal, under high ALWC conditions. Overall, these results

441   demonstrate that the observed aqSOA could be formed predominantly from

442 biomass-burning emissions through aqueous-phase reactions, reinforcing the

443 important role of BBOA in increasing PM$_{2.5}$ mass concentration.
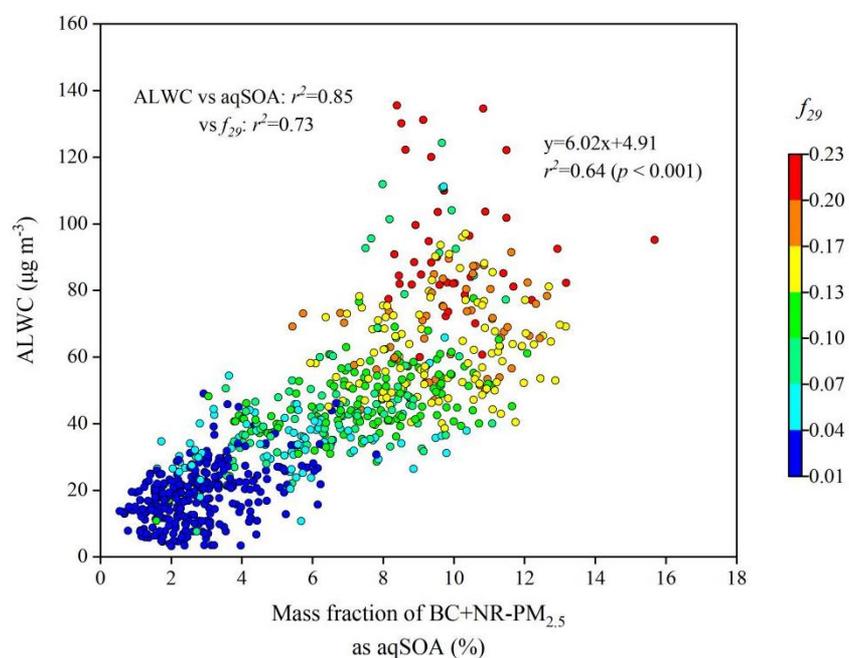
444

445 **Figure 3.** Scatter plot of the mass fraction of aqSOA in BC + NR-PM$_{2.5}$ versus ALWC, coloured

446 by f_{29} (normalized signal at m/z 29) during the campaign. f_{29} (mainly CHO$^+$) is a tracer for alcohol

447 compounds and is used to monitor the aqueous-phase oxidation of organic compounds, such as

448 glyoxal.
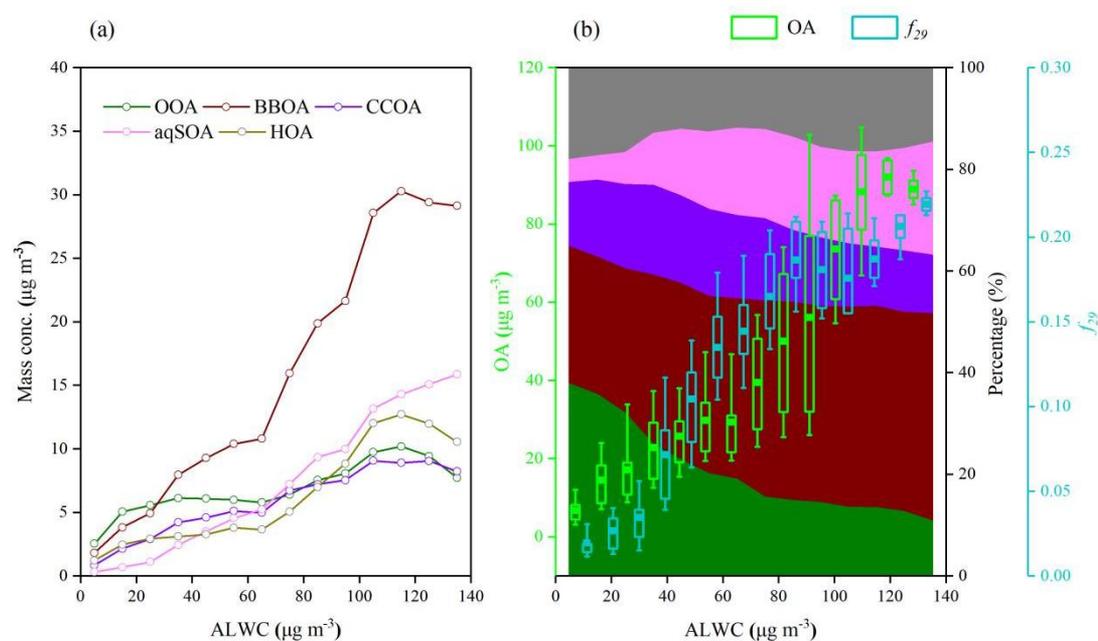
449

450 **Figure 4.** Variations of **(a)** OA factor mass concentrations, **(b)** OA mass concentrations, f_{29} (a

451 tracer for alcohol compounds), and mass fraction of OA factors as a function of ALWC. Data were

452   grouped into different bins according to a 10-µg m^{-3} increment of ALWC.

453   To identify the formation of aqSOA and its precursors under different PM$_{2.5}$

454   pollution levels, the relationships between aqSOA and BBOA or OOA mass

455   concentrations, as well as key ion-fragment tracers, were analyzed separately during

456   CP and PP. The correlation (r^2) between aqSOA and BBOA was stronger during PP

457   (0.64) than during CP (0.54) ($p < 0.001$, Fig. 5a, c). Although both aqSOA and BBOA

458   concentrations increased with increasing ALWC during both periods, the correlations

459   of ALWC with aqSOA and BBOA were relatively stronger during PP than during CP

460   ($p < 0.001$). As shown in Fig. 5b, d, f_{29} was highly correlated with aqSOA formation

461   during both CP and PP. A subset of data points with high aqSOA and OOA

462   concentrations displayed relatively low f_{29} values (0.071−0.102), as shown in Fig. 5d.

463   For these points, the average value of f_{44} (normalized signal of m/z 44) (0.103 ± 0.024)

464   was 1.3 times that of the overall dataset (0.080 ± 0.035) during PP, likely due to the

465   formation of more-oxidized OOA under high ALWC values (> 80 µg m^{-3}) (Xu et al.,

466   2017). Previous studies have found that f_{29} values for polyols and species with

467   non-acid OH groups from biomass-burning emissions were typically lower than 0.15

468   (Canagaratna et al., 2015; Gilardoni et al., 2016; Zhao et al., 2014). Moreover, the

469   mass fraction of aqSOA showed a stable increasing trend and remained elevated (from

470   18% to 22%) at ALWC > 80 µg m^{-3}, accompanied by a corresponding decrease in

471   OOA (from 15% to 10%) (Fig. 4b). In contrast to OOA ($p > 0.1$), aqSOA

472   concentration showed a strong positive correlation with ALWC ($r^2 = 0.73$, $p < 0.001$)

473   when ALWC > 80 µg m^{-3} during PP. However, no such correlations were observed

474   during CP ($p > 0.1$). Notably, a strong anticorrelation between aqSOA and OOA

475   concentrations was observed during PP at ALWC > 80 µg m^{-3} when $f_{29} > 0.15$ ($r^2 =$

476   0.76, $p < 0.001$), but not during CP ($p > 0.1$) (Fig. 5b, d). These results indicated that

477   aqSOA formation was more intensive than OOA at high ALWC levels during PP.

478   Previous research demonstrated that f_{44} could be used as a tracer for aged SOA,

479   f_{43} (normalized signal at m/z 43) for POA and fresh SOA, and f_{60} (presence of

480   anhydrosugars) for BBOA (Cubison et al., 2011; Ng et al., 2010). Additionally, m/z 44

481   and 43 are typically from different functional groups, and their ratio changes as a

function of atmospheric aging. The triangle plot of f_{44} versus f_{43} has been widely used to characterize OA evolution, whereas that of f_{44} versus f_{60} is commonly used to track the aging of BBOA (Ortega et al., 2013; Paglione et al., 2020; Xu et al., 2017; Xu et al., 2019). In this study, the bottom region of the triangle (Fig. 6) was dominated by BBOA, CCOA, and HOA, which exhibited low f_{44} (0.040, 0.017, and 0.016, respectively), indicating fresh, less-oxidized emissions. In contrast, the f_{44} of SOA factors (OOA and aqSOA; 0.118 and 0.117, respectively) were observably higher, reflecting their oxidized nature. The f_{44} of aqSOA was close to that observed in fog (Gilardoni et al., 2016; Kim et al., 2019), highlighting the role of aqueous-phase reactions in this study. Moreover, the relative abundance of m/z 45 (mainly HCO_2^+), a tracer ion for carboxylic acids, was higher in the aqSOA spectrum than in the OOA spectrum (Fig. S9), consistent with previous findings that aqueous-phase reactions are important sources of oxygenated organic compounds, including organic acids (Ervens et al., 2011; Kim et al., 2019; McNeill, 2015; Sun et al., 2010; Yu et al., 2014). As shown in Fig. 6b, BBOA and aqSOA displayed higher f_{60} values (0.019 and 0.011, respectively) than CCOA (0.009) and HOA (0.008). The f_{60} value of OOA was 0.002, which is lower than the typical background level (0.003) observed in the atmosphere unaffected by biomass burning (Cubison et al., 2011). The mass spectrometry feature of aqSOA, characterized by elevated f_{44} and f_{60} values, placed it in the schematic region of aged BBOA reported in previous studies (Cubison et al., 2011; Ortega et al., 2013). Additionally, BBOA contains abundant water-soluble organic compounds, such as sugars, phenols, and organic acids, that can efficiently form aqSOA through aqueous-phase reactions, such as oxidation and oligomerization reactions (Ervens et al., 2011; Gilardoni et al., 2016; Lee et al., 2013; Lei et al., 2024; Li et al., 2020; Powelson et al., 2014). In contrast, OOA formation primarily relies on the gas-phase oxidation of VOCs with high-reactivity, such as aromatics and long-chain alkanes, by OH radicals, which have low concentrations in BBOA plumes (Akagi et al., 2011; Jimenez et al., 2009; Shrivastava et al., 2017; Yokelson et al., 2007). This suggests that BBOA acts as an important precursor for aqSOA instead of OOA through aqueous-phase reactions. These results are consistent with previous studies, and most

删除[Chao]: ic

20

512 of the observed data fall within the triangle space (Bao et al., 2023; Kim et al., 2019;

513 Paglione et al., 2020). Notably, aqSOA formation processes can be more intense and

514 significant during autumn due to elevated precursor concentrations (e.g., BBOA),

515 ALWC, and RH values, though the underlying chemical pathways are robust and can

516 occur year-round (Bao et al., 2023; Tang et al., 2025; Zeng et al., 2025).

517 During PP, f_{44} values ranging from 0.022 to 0.140 (0.080 ± 0.035) were

518 significantly higher than those during CP (0.021−0.150, 0.064 ± 0.019) ($p < 0.001$),

519 whereas f_{43} was slightly lower, with an average of 0.062 ± 0.027. Compared with CP

520 ($r^2 = 0.17$, slope = −0.53), f_{44} showed a more pronounced inverse relationship with f_{43}

521 during PP, characterized by a higher r^2 value (0.70) and a regression slope closer to −1

522 (−1.09). This pattern indicated a greater abundance of aged SOA in the atmosphere

523 during PP (Fig. 6a and c). Notably, data points in the $f_{44} - f_{43}$ space during PP fell

524 within the upper boundary of the triangle region, with most points located outside the

525 bottom boundary. These results suggested that less oxidized SOA was predominantly

526 formed through aqueous-phase processing, instead of gas-phase photochemical

527 oxidation, during PP (Kim et al., 2019; Zhao et al., 2019). Moreover, points outside

528 the bottom boundary of the triangle region, characterized by higher f_{44} (> 0.05) and

529 lower f_{43} (< 0.06), were associated with relatively higher ALWC during PP, a feature

530 not observed during CP.

531 Here, the triangle plots of f_{44} versus f_{60}, coloured by ALWC under different PM$_{2.5}$

532 pollution levels, were analyzed (Fig. 6b, d), while the link between aqSOA and BBOA

533 was further stressed by a schematic representation of aged BBOA. Except for a few

534 outliers, f_{60} values were consistently higher than 0.003, and most data points fell

535 within the triangular region, suggesting a widespread influence of biomass burning on

536 OA. During PP, f_{60} ranged from 0.005 to 0.019 (0.010 ± 0.004), similar to the range

537 observed in CP (from 0.004 to 0.019, 0.010 ± 0.003). However, the correlation

538 between f_{44} and f_{60} was higher during PP ($r^2 = 0.72$) than during CP ($r^2 = 0.31$) ($p < $

539 0.001). Moreover, data points within the schematic space of aged BBOA showed

540 relatively higher ALWC compared with the overall dataset during PP, a pattern that

541 was not evident during CP.

删除[Chao]: m

删除[Chao]: reactions

删除[Chao]: photochemical pathways

542   Regional transport significantly influenced the aging of BBOA in the SCB.

543   Previous studies have demonstrated that northeast winds prevail during autumn in this

544   region, facilitating the transport of pollutants along the Dazhou→Guang'an→Hechuan

545   pathway, and this northeast-southwest transport pathway had a significant impact on

546   Chongqing (Peng et al., 2019; Wang et al., 2018). As shown in Fig. S11, air masses

547   during the campaign predominantly originated from northeastern Chongqing, an area

548   with widespread agricultural burning activities (He et al., 2015; Luo et al., 2020), and

549   were transported over relatively short distances. Compared to other air mass clusters,

550   the highest contribution and concentration of BBOA to total $PM_{2.5}$ were observed

551   when air masses passed through northeastern Chongqing. The percentage of air mass

552   trajectories that passed through biomass-burning-influenced regions was higher

553   during PP (~57%) than during CP (~35%). Unlike Cluster 3 during CP, air masses

554   originating from northeastern Chongqing (Cluster 2) during PP showed significantly

555   higher contributions and concentrations of BBOA (24.7%, 27.8 µg m^{-3}) and aqSOA

556   (9.4%, 10.6 µg m^{-3}) than other clusters ($p < 0.001$). In addition, Cluster 2 exhibited

557   notably higher values of ALWC (93.7 µg m^{-3}), $Abs_{370,BrC,sec}$ (105.1 Mm^{-1}), f_{44} (0.113),

558   and the NO_3/SO_4 ratio (2.1, a tracer for BBOA aging (Liu et al., 2024; Zhang et al.,

559   2025)) than other clusters during PP ($p < 0.001$). During PP, approximately 68% of

560   the trajectories in Cluster 2 passed through biomass-burning-influenced regions, with

561   transport times to the sampling site ranging from 12 to 48 h, consistent with the

562   typical timescale for aqueous-phase aging of biomass-burning emissions reported in

563   earlier works (Cubison et al., 2011; Hennigan et al., 2010; Ortega et al., 2013; Zhu et

564   al., 2023). These results suggest that regionally transported BBOA, primarily

565   originating from northeastern Chongqing, underwent aging to form aqSOA within

566   approximately 12–48 h.
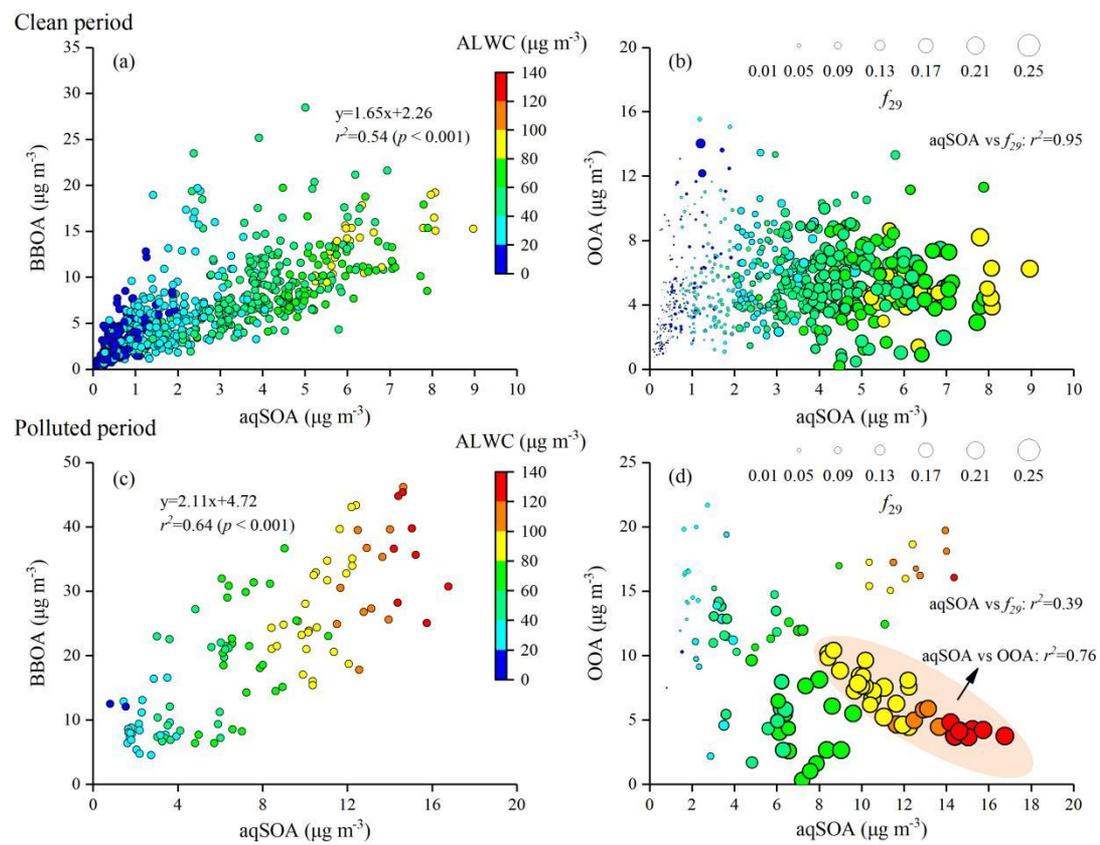
Figure 5. Scatter plots of aqSOA versus **(a, b)** BBOA and **(c, d)** OOA mass concentrations, coloured by ALWC during CP and PP. The size of the symbols panel in **(b)** and **(d)** increases with the increase in the f_{29} value, which is a tracer for alcohol compounds.
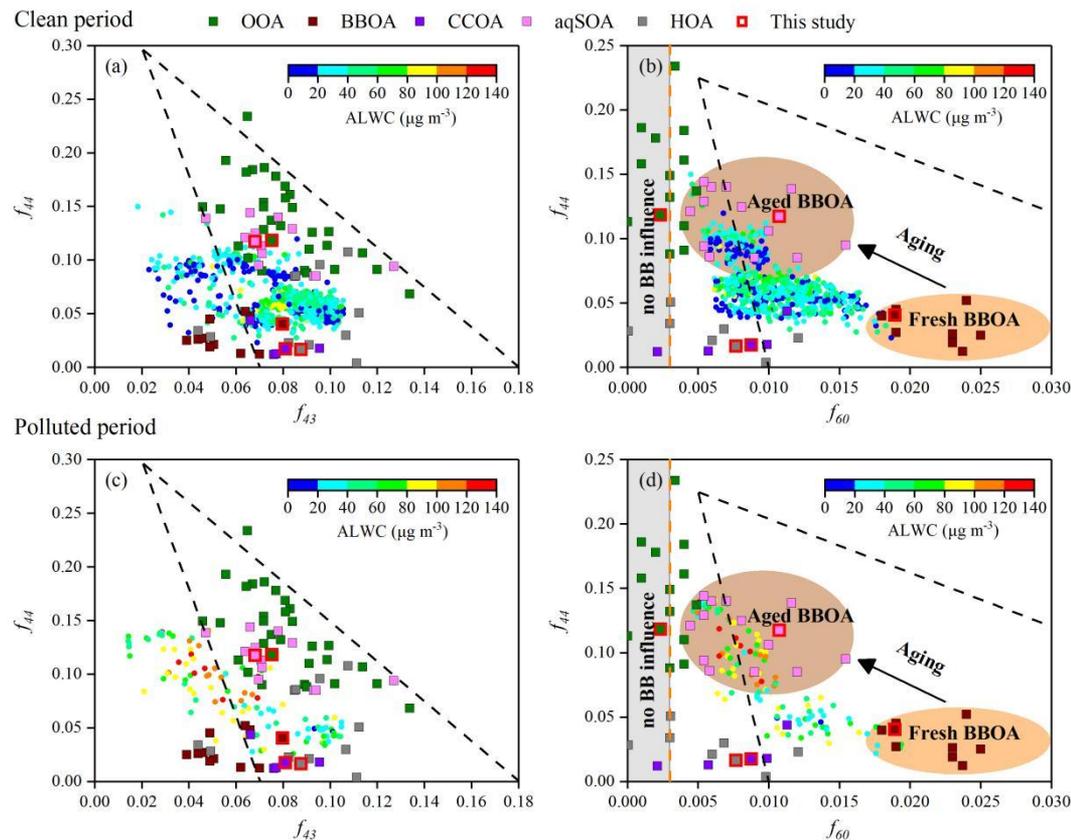
Figure 6. Triangle plots of **(a, c)** f_{44} (normalized mass spectrum signal at m/z 44) versus f_{43} (normalized mass spectrum signal at m/z 43) and **(b, d)** f_{44} versus f_{60} (normalized mass spectrum signal at m/z 60), coloured by ALWC (circles) during CP and PP. The dashed lines in **(a)** and **(c)** were derived from Ng et al. (2010) and used to follow the aging of OA components in the atmosphere. The background space ($f_{60} < 0.003$) without biomass burning influence is also shown by the grey shaded area. The background value of secondary aged OA (brown dashed line) and the black dashed lines characterizing the aging of BBOA in **(b)** and **(d)** were derived from Cubison et al. (2011). The data points (squares) included the measurements from this study (bordered in red) and previous research (Bao et al., 2023; Gilardoni et al., 2016; Kim et al., 2019; Ng et al., 2011a; Paglione et al., 2020; Xu et al., 2015; Xu et al., 2017; Xu et al., 2019; Zhao et al., 2017; Zhao et al., 2019). f_{43} (mainly $C_2H_3O^+$) is a tracer for POA and fresh SOA; f_{44} is a proxy of the OA oxygenation degree and used as a tracer for aged SOA; and f_{60} is a proxy of anhydrosugars emitted from biomass burning.

删除[Chao]: was

3.3 Evolution of BrC Absorption

Previous research indicates that OA from both fresh and aged biomass-burning emissions exhibits light absorption across the UV–Vis range, with significantly higher AAE values than BC, and may contribute to net positive radiative forcing (Laskin et al., 2015). In this study, the absorption properties of BrC and their relationships with the five OA factors were analyzed. The values of $Abs_{\lambda,BrC,pri}$ and $Abs_{\lambda,BrC,sec}$ were obtained using the MRS method, and the Abs value of each OA factor at each wavelength was estimated using the MLR method (SI Text S3 and S4). The mean $Abs_{370,BrC}$ was 42.4 ± 28.5 Mm^{-1} (accounting for 49.2% of Abs_{370}), much higher than $Abs_{660,BrC}$ (2.6 ± 1.3 Mm^{-1}, 10.5%), suggesting high absorption efficiency for BrC in the near-UV region. From 370 to 660 nm, $Abs_{\lambda,BrC,pri}$ and $Abs_{\lambda,BrC,sec}$ accounted for 56.8%−72.5% and 27.5%−43.2% of $Abs_{\lambda,BrC}$, respectively, indicating that primary emissions were the dominant contributors to BrC absorption (Fig. S13). However, the contribution of $Abs_{\lambda,BrC,sec}$ to $Abs_{\lambda,BrC}$ increased with wavelength, suggesting that the impact of SOA on Abs_{BrC} should not be ignored. The following analysis demonstrates that aqSOA formed from aged BBOA contributed substantially to the BrC budget and exhibited strong light absorption across the UV–Vis range.

Data at 370 nm, which exhibit higher SNRs and a greater contribution of Abs_{BrC}, were selected to further analyze the correlations of BrC absorption with various OA components. As described in Section 2.3.3, the Abs of the five OA factors at each wavelength were obtained using the MLR method (Table S2). The contributions of BBOA ($Abs_{370,BBOA}$) and aqSOA ($Abs_{370,aqSOA}$) to $Abs_{370,BrC}$ were 51.9% and 16.4%, respectively, exceeding those of CCOA (11.5%), HOA (9.1%), and OOA (11.1%). This pattern is consistent with the higher MAC values of BBOA and aqSOA (Fig. S15).

Figure S16 presents correlations between $Abs_{370,BrC}$ and the mass concentrations of OOA, BBOA, CCOOA, aqSOA, HOA, and the tracer ion m/z 60 (ion fragment tracers of BBOA). $Abs_{370,BrC}$ exhibited the strongest positive correlations with BBOA and m/z 60 ($r^2 = 0.77$, $p < 0.001$), followed by aqSOA ($r^2 = 0.69$, $p < 0.001$). In

contrast, correlations with HOA ($r^2 = 0.36$), CCOA ($r^2 = 0.25$), and OOA ($r^2 = 0.09$, $p > 0.1$) were much weaker. Among all OA factors (excluding BBOA), aqSOA contributed relatively more to $Abs_{370,BrC}$ (Table S2) and also displayed a stronger correlation with $Abs_{370,BrC}$. These results may be related to the formation of aqSOA from aged BBOA via aqueous-phase reactions. Gilardoni et al. (2016) demonstrated that aqSOA derived from aged BBOA through aqueous-phase reactions. Gilardoni et al. (2016) demonstrated that aqSOA derived from aged BBOA through aqueous-phase reactions in the ambient atmosphere contributes to the BrC budget and exhibits slightly higher $AAE_{467-660}$ (AAE of aerosols from 467 to 660 nm) values than fresh or processed biomass-burning emissions in laboratory experiments.

The MAC values of the five resolved OA components (equivalent to coefficients a–e in the MLR method) at different wavelengths are shown in Fig. S15.

删除[Chao]: were

At 370 nm, BBOA showed the highest MAC (2.37 m^2 g^{-1}), followed by aqSOA (1.23 m^2 g^{-1}), indicating that oxidation of BBOA to aqSOA reduces light absorption at shorter wavelengths. Previous research found that the MAC of BBOA at 365 nm is twice that of SOA, which was associated with water-soluble BrC (Lorenzo et al., 2017; Washenfelder et al., 2015). The AAE values of the OA factors, calculated by a power-law fitting of their Abs from 370 nm to 660 nm (Qin et al., 2018; Wang et al., 2019b), are shown in Fig. S15. Notably, aqSOA had the lowest $AAE_{370-660,aqSOA}$ value

删除[Chao]: were

(3.54), whereas BBOA had the highest $AAE_{370-660,BBOA}$ value (4.93). Moreover, the contribution of aqSOA to Abs_{BrC} increased from 16.4% at 370 nm to 26.7% at 660 nm, whereas that of BBOA decreased from 51.9% to 39.1% over the same wavelength range. These findings suggest that aqSOA formed from aged BBOA significantly contribute to the light absorption of BrC in the UV–Vis range.

Figure 7 shows a ternary contour map that quantifies the contributions of BBOA, CCOA, and HOA to $Abs_{370,BrC,pri}$. A strong positive correlation ($p < 0.001$) and a steep linear regression slope (1.80) were observed between the BBOA mass concentration and $Abs_{370,BrC,pri}$. Among these POA factors, high mass fractions of BBOA relative to POA were consistent with high values of $Abs_{370,BrC,pri}$ (Fig. 7a). For example, most data points with $Abs_{370,BrC,pri}$ higher than 49.1 Mm^{-1} (90th percentile of $Abs_{370,BrC}$) fell

within the region of high BBOA/POA values (> 0.5). Moreover, $Abs_{370,BrC,pri}$ increased significantly with increasing BBOA and m/z 60 mass concentrations, exhibiting higher correlation coefficients ($r^2 = 0.63$ and 0.55) than HOA ($r^2 = 0.19$) and CCOA ($r^2 = 0.14$) (Fig. 7b). These results indicate the major contribution of BBOA to primary BrC light absorption at 370 nm.

To understand the relationship between secondary BrC absorption and its chromophores, the correlation between $Abs_{370,BrC,sec}$ and the mass concentrations of SOA factors was analyzed. As shown in Fig. S17, $Abs_{370,BrC,sec}$ increased significantly with increasing aqSOA concentration ($r^2 = 0.44$, $p < 0.001$), and high $Abs_{370,BrC,sec}$ values were associated with elevated ALWC. In contrast, no such relationship was found for OOA ($p > 0.1$). The slope of the linear regression between aqSOA mass concentrations and $Abs_{370,BrC,sec}$ (3.50) was steeper than that for OOA (Fig. S17), and the MAC values of aqSOA were also higher across the UV–Vis range (Fig. S15).

To further characterize the evolution of secondary BrC absorption, $Abs_{370,BrC,sec}$ was normalized by ΔCO (background-corrected CO mixing ratios) to minimize the effect of boundary layer height (Fig. 8) (DeCarlo et al., 2010). Here, the background CO value (400 ppb) was defined as the lowest 1.25th percentile of CO values during the campaign (Kondo et al., 2006). Figure 8 shows that the ratios of $Abs_{370,BrC,sec}/\Delta CO$ increased with both aqSOA concentration and ALWC from 17:00 to 03:00 LT ($r^2 = 0.63$, 0.57, $p < 0.001$), whereas $Abs_{370,BrC,pri}/\Delta CO$ decreased slightly with increasing BBOA and m/z 60 concentrations over the same period ($r^2 = 0.35$, 0.33, $p < 0.001$). Additionally, the average concentrations of NO_3, NH_4, and NO_2 from 17:00 to 03:00 LT (9.1 μg m^{-3}, 5.6 μg m^{-3}, and 16.0 ppb, respectively) were 1.2, 1.2, and 1.3 times those from 04:00 to 16:00 LT (7.7 μg m^{-3}, 4.7 μg m^{-3}, and 12.6 ppb, respectively). These results are consistent with previous winter observations in the SCB (Peng et al., 2025; Wu et al., 2024).

As discussed in Section 3.2, SOA with hydroxyl groups, such as glyoxal and methylglyoxal, can form from aged BBOA through aqueous-phase reactions under high ALWC. Previous studies have shown that oligomers formed through aqueous reactions of glyoxal with NH_3, which contain C=C or C=N bonds, exhibit strong

删除[Chao]: mass

删除[Chao]: (involving two glyoxal molecules)

27

absorption in near-UV regions (Laskin et al., 2015; Lee et al., 2013; Nozière et al., 2009; Powelsonet al., 2014). This suggested that secondary BrC chromophores with strong absorption at 370 nm were formed under high ALWC from 17:00 to 03:00 LT, which may be related to aqSOA generated from aged BBOA through aqueous-phase reactions. The low values of $Abs_{370,BrC,sec}/\Delta CO$ from 12:00 and 14:00 LT may be related to photolysis and/or photooxidation causing BrC photobleaching (Sareen et al., 2013; Zhao et al., 2015). Overall, our findings suggest that aqSOA formed from biomass-burning emissions contributed significantly to BrC absorption, especially at night during the campaign.

Previous studies indicate that biomass-burning activity is negligible in summer, and although it may also occur in spring and winter, its intensity is typically lower than in autumn (Chen et al., 2014; Chen et al., 2017; Tao et al., 2014; Yang et al., 2019). Tao et al. (2014) reported that biomass burning contributed $19 \pm 11\%$ to $PM_{2.5}$ during autumn, significantly higher than in other seasons, and accounted for the highest fraction of organic matter in $PM_{2.5}$. Additionally, the concentration of BBOA and its fraction in OA during autumn in this study (8.6 ± 7.7 μg m^{-3} and $34.8 \pm 11.2\%$, respectively) were respectively higher than those observed during summer (0.41 μg m^{-3} and 5.7%, respectively) (Zeng et al., 2025) and winter in the SCB (Tang et al., 2025; Zhang et al., 2023) (Table S1). Notably, the ALWC during autumn in this study (41.6 ± 24.9 μg m^{-3}) was substantially higher than that reported for summer (18.6 ± 35.3 μg m^{-3}; Zeng et al., 2025) and winter (27.4 ± 9.7 μg m^{-3}; Tang et al., 2025) in the SCB. Wang et al. (2018) observed that RH values at Chengdu and Chongqing in autumn were also higher than those in other seasons. Previous research indicates that, while aqueous-chemistry pathways in spring were comparable to those in autumn, photochemical bleaching of BrC was potentially stronger in spring (Wang et al., 2019a). Although winter features lower biomass-burning emissions, secondary BrC could still form from BBOA through aqueous-phase reactions under high NO_x and NH_4 concentrations and stagnant nighttime conditions, as observed during winter in the SCB (Peng et al., 2025; Wu et al., 2024). In summer, elevated temperature and O_x ($O_x = NO_2 + O_3$) levels could enhance photochemical oxidation, promoting secondary

BrC formation while also intensifying BrC photobleaching (Wu et al., 2024). In summary, while secondary BrC can derive from BBOA through aqueous-phase reactions in all seasons in the SCB (with the possible exception of spring), the elevated ALWC and BBOA concentrations during autumn are favourable for its aqueous-phase formation.

$AAE_{370-880}$ is another key parameter for characterizing aerosol absorption properties. Figure 9 displays its correlations with the mass fraction of aqSOA (f_{aqSOA}) and BBOA (f_{BBOA}) to OA and the BC-to-OA ratio. During the campaign, a strong positive correlation ($r^2 = 0.49$, $p < 0.001$) was observed between $AAE_{370-880}$ and f_{aqSOA}, with $AAE_{370-880}$ reaching values up to 2.65. In contrast, $AAE_{370-880}$ increased only slightly with increasing f_{BBOA} ($r^2 = 0.21$, $p < 0.001$) (Fig. 9a, c). AAE was calculated using a power-law fitting of aerosol absorption values (Qin et al., 2018; Wang et al., 2019b). While BC concentration was linearly dependent on Abs_{BC}, OA concentration did not follow the same pattern with Abs_{BrC}. The mixing state of BC and OA, influenced by combustion conditions, can also affect AAE. Previous studies have shown that biomass-burning emissions can impact absorption properties, which is reflected in the relationship between AAE and the BC-to-OA ratio (a measure of the combustion conditions) (Lu et al., 2015; Saleh et al., 2014). Thus, the relationship observed in Fig. 9b reflects the influence of biomass-burning emissions during this campaign. The parameterised curve (black) agrees with prior research (red) for wavelengths from 370 to 880 nm (Lu et al., 2015). When 950 nm was used as the highest wavelength instead of 880 nm, $AAE_{370-950}$ values differed by less than 10% from $AAE_{370-880}$. Notably, data points with high $AAE_{370-880}$ corresponded to low BC-to-OA ratios and large f_{aqSOA} values. Moreover, the average value of $AAE_{370-880}$ observed in this study (1.95) was higher than $AAE_{370-950}$ observed in the laboratory experiments on fresh and photochemically aged biomass-burning emissions (i.e., 1.38 and 1.48 for fresh oak and pocosin pine, and 1.42 and 1.73 for aged oak and pocosin pine) (Saleh et al., 2013).
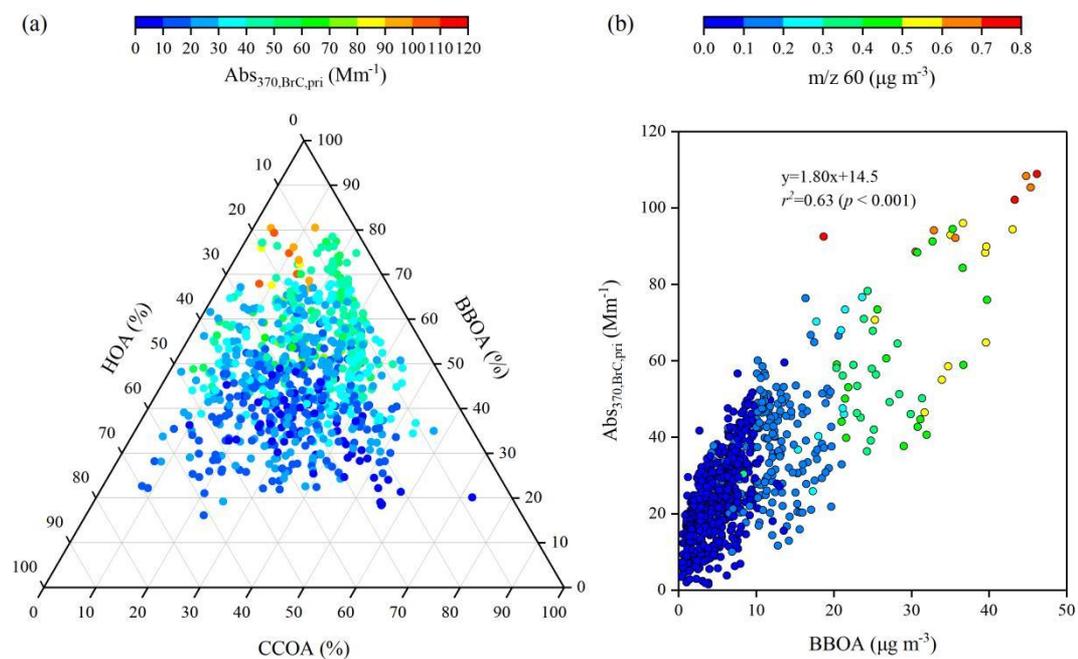
732

733 **Figure 7. (a)** Ternary diagram for the mass fractions of BBOA, CCOA, and HOA in POA,

734 coloured by $Abs_{370,BrC,pri}$, and **(b)** scatter plot of BBOA mass concentrations versus $Abs_{370,BrC,pri}$,

735 coloured by m/z 60 mass concentrations.
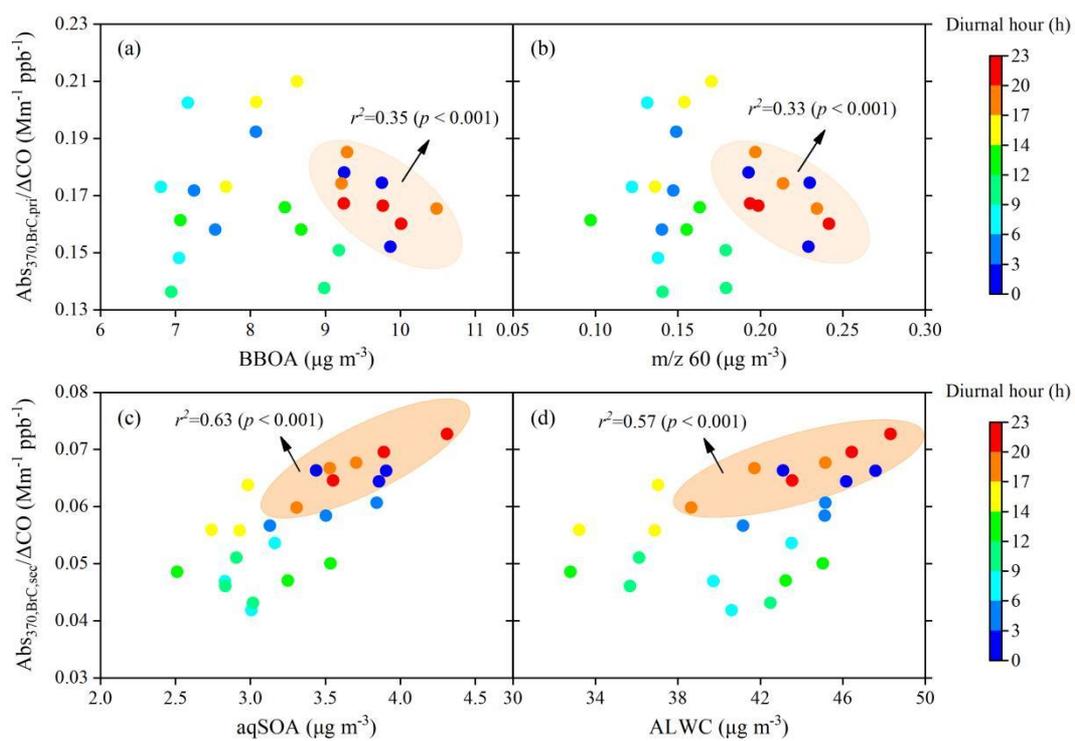
736

737 **Figure 8.** Scatter plots of $Abs_{370,BrC,pri}/\Delta CO$ versus **(a, b)** BBOA and m/z 60 mass concentrations

738 and $Abs_{370,BrC,sec}/\Delta CO$ versus **(c, d)** aqSOA and ALWC, coloured by the local time.
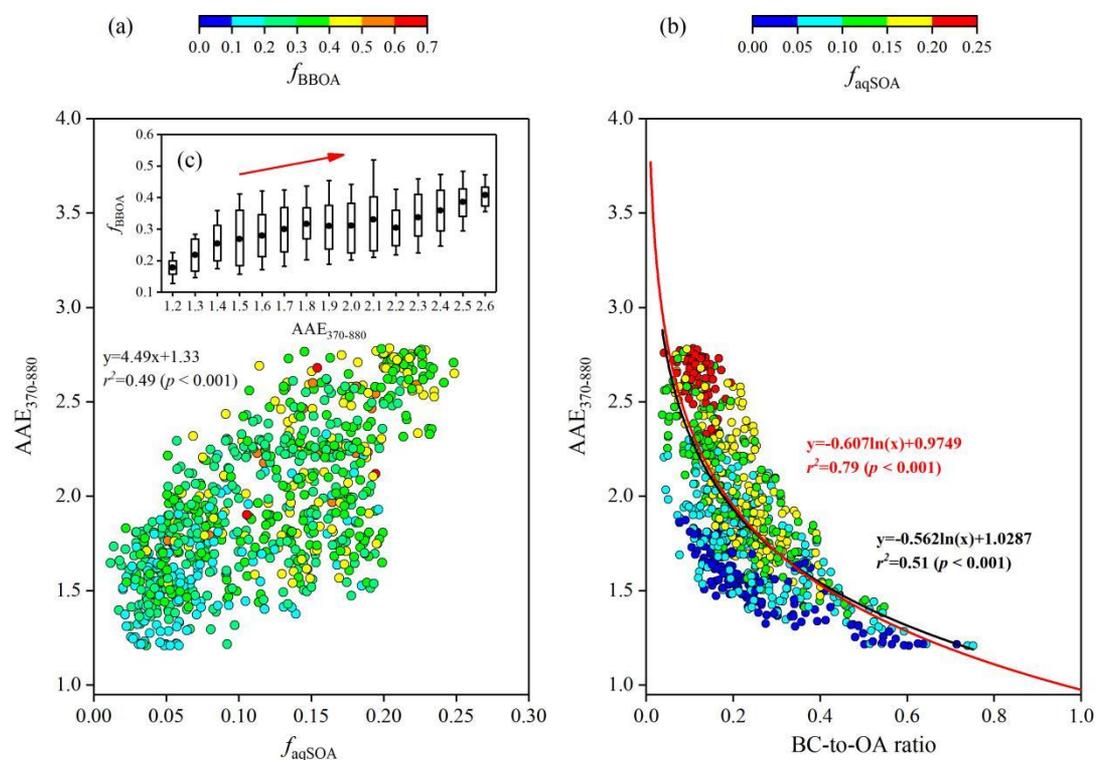
739

740 **Figure 9.** Relationship between **(a)** $AAE_{370-880}$ and the mass fraction of aqSOA (f_{aqSOA} =

741 aqSOA/OA), coloured by the mass fraction of BBOA (f_{BBOA} = BBOA/OA), and **(b)** BC-to-OA

742 ratios coloured by f_{aqSOA}. **(c)** Variations of f_{BBOA} as a function of $AAE_{370-880}$. The red curve in **(b)**

743 was the best fit curve to data taken from Lu et al. (2015) and described the Abs of fresh and aged

744 BBOA.

4 Conclusions

746   This study conducted comprehensive real-time measurements of the light

747 absorption properties and chemical composition of carbonaceous aerosols during

748 autumn in the Sichuan Basin, China. The findings demonstrated that aqueous

749 secondary organic aerosol (aqSOA) formed from aged biomass-burning emissions

750 under high aerosol liquid water content (ALWC > 60 μg m^{-3}) conditions significantly

751 contributes to aerosol pollution and light absorption. OA was the dominant component

31

of PM$_{2.5}$ (46.6 ± 10.7%) and exhibited strong absorption at UV wavelengths (Abs$_{370,BrC}$ = 42.4 ± 28.5 Mm^{-1}). During PP, aqSOA contributed, on average, 14.1% to OA (7.6 µg m^{-3}), exhibiting enhanced oxidation (f_{29} = 0.141 ± 0.062, f_{44} = 0.080 ± 0.035) and substantial light absorption characteristics (Abs$_{370,BrC}$ = 91.6 Mm^{-1}, AAE$_{370-880}$ = 2.1). Additionally, less-oxidized aqSOA, formed predominantly through aqueous-phase reactions, instead of gas-phase photochemical oxidation of their precursors, significantly contributed to the dynamic evolution of haze pollution during PP. Backward trajectory analysis further revealed that regionally transported BBOA, which originated primarily from northeastern Chongqing, underwent aqueous-phase aging to aqSOA within approximately 12–48 h. These results underscore that aqueous-phase reactions of BBOA—particularly during the transport of biomass-burning plumes—convert primary emissions into strongly light-absorbing aqSOA, thereby substantially influencing regional haze formation and radiative forcing.

Our findings align with previous laboratory studies on biomass-burning BrC formation, and provide novel ambient quantification of these processes under realistic atmospheric conditions. The parameterized curve of AAE$_{370-880}$ versus BC-to-OA ratios in this study was consistent with previous laboratory research on biomass-burning emissions. The mean AAE$_{370-880}$ observed in this study (1.95) was higher than the values reported for fresh and photochemically aged biomass-burning emissions in laboratory experiments, and increased significantly with increasing f_{aqSOA} (r^2 = 0.49, p < 0.001). Additionally, elevated Abs$_{370,BrC,sec}$ values coincided with high ALWC, NO$_3$, and NH$_4$ levels and correlated strongly with aqSOA concentration (r^2 = 0.44, p < 0.001). These results suggest that aqueous-phase reactions of BBOA under high-NO$_x$ and high-NH$_4$ conditions produce secondary BrC with particularly strong light absorption. Notably, seasonal variations in biomass-burning emissions and the associated chemical processing of carbonaceous aerosols must be adequately represented in climate and air quality models. Conducting the campaign in autumn, when biomass-burning activity is intense, is critical to avoid underestimating aerosol impacts in this season and overestimating them in other seasons. However, the results

782 may not fully represent aerosol processes in other seasons. The relative uncertainty of

783 Abs_{BrC} at 370 nm, resulting from the choice of AAE_{BC}, ranged from -112% to 42%.

784 Nevertheless, our results underscore the importance of aqueous-phase processing in

785 transforming biomass-burning emissions, with important implications for climate and

786 air quality modelling. The substantial contribution of aqSOA to aerosol mass and light

787 absorption highlights the requirement for improved representation of aqueous

788 processes in models. The linkages established here among aging timescales, transport

789 pathways, and aqSOA formation provide a transferable framework for understanding

790 aqSOA processing in other humid regions influenced by biomass burning. Research

791 on BrC chromophores is still in its early stages, and quantitative linking their

792 chemical composition and light absorption properties to biomass-burning emissions

793 across different seasons are necessary to improve our understanding of their climatic

794 and environmental effects. Future research should prioritize molecular-level

795 characterization of aqSOA precursors and products, quantification of aqueous reaction

796 rates under ambient conditions, and multi-scale modelling to assess regional climate

797 impacts. This study highlights that aqueous processes play an important role in the

798 evolution of biomass-burning emissions and should be adequately considered in both

799 air quality budgets and climate forcing balance on a global scale.

800

801 **Data availability.** The data generated and analysed in this study are available from

802 https://doi.org/10.5281/zenodo.18635386 (Peng et al., 2026).

803

804 **Author contributions.** CZ, CP, YD, and ZL designed the experiments. Data analysis

805 and interpretation were performed by CP, ZT, HT, KZ, ZL, and GS. CP, XY, and MT

806 wrote the paper. ZT, YC, XL, LZ, YC, and YF contributed to the paper with useful

807 scientific discussions or comments.

808

809 **Competing interests.** The authors declare that they have no conflict of interest.

810

References

Akagi, S. K., Yokelson, R. J., Wiedinmyer, C., Alvarado, M. J., Reid, J. S., Karl, T., Crounse, J. D., and Wennberg, P. O.: Emission factors for open and domestic biomass burning for use in atmospheric models, Atmos. Chem. Phys., 11, 4039−4072, https://doi.org/10.5194/acp-11-4039-2011, 2011.

Alfarra, M. R., Prévôt, A. S. H., Szidat, S., Sandradewi, J., Sandradewi, S., Lanz, V. A., Schreiber, D., Mohr, M., and Baltensperger, U.: Identification of the Mass Spectral Signature of Organic Aerosols from Wood Burning Emissions, Environ. Sci. Technol., 41, 5770−5777, https://doi.org/10.1021/es062289b, 2007.

Bahreini, R., Ervens, B., Middlebrook, A. M., Warneke, C., de Gouw, J. A., DeCarlo, P. F., Jimenez, J. L., Brock, C. A., Neuman, J. A., Ryerson, T. B., Stark, H., Atlas, E., Brioude, J., Fried, A., Holloway, J. S., Peischl, J., Richter, D., Walega, J., Weibring, P., Wollny, A. G., and Fehsenfeld, F. C.: Organic Aerosol Formation in Urban and Industrial Plumes Near Houston and Dallas, Texas, J. Geophys. Res.: Atmos., 114, D00F16, doi:10.1029/2008JD011493, 2009.

Bao, Z. E., Liu, Y. L., Meng, L. S., Han, Y., Tian, M., Shi, G. M., Wang, Q. Y., Huang, Y., Peng, C., Luo, B., Zhang, W., Wang, H. B., Cao, J. J., Yang, F. M., and Chen, Y.: Evaluating the effects of biomass burning on severe haze formation in a megacity of Sichuan Basin, Southwestern China, J. Geophys. Res.: Atmos., 130, e2024JD042516, https://doi.org/10.1029/ 2024JD042516, 2025.

Bao, Z. E., Zeng, X. L., Zhou, J. W., Yang, F. M., Lu, K. D., Zhai, C. Z., Li, X., Feng, M., Tan, Q. W., and Chen, Y.: Evolution of black carbon and brown carbon during summertime in Southwestern China: An assessment of control measures during the 2023 Chengdu Summer World University Games, Environ. Pollut., 357, 124467, https://doi.org/10.1016/j.envpol.2024.124467, 2024.

Bao, Z. E., Zhang, X. Y., Li, Q., Zhou, J. W., Shi, G. M., Zhou, L., Yang, F. M., Xie, S. D., Zhang, D., Zhai, C. Z., Li, Z. L., Peng, C., and Chen, Y.: Measurement report: Intensive biomass burning emissions and rapid nitrate formation drive severe haze formation in the Sichuan Basin, China – insights from aerosol mass spectrometry, Atmos. Chem. Phys., 23, 1147−1167, https://doi.org/10.5194/acp-23-1147-2023,

845   2023.

846   Canagaratna, M. R., Jayne, J. T., Jimenez, J. L., Allan, J. D., Alfarra, M. R., Zhang, Q.,

847   Onasch, T. B., Drewnick, F., Coe, H., Middlebrook, A., Delia, A., Williams, L. R.,

848   Trimborn, A. M., Northway, M. J., DeCarlo, P. F., Kolb, C. E., Davidovits, P., and

849   Worsnop, D. R.: Chemical and microphysical characterization of ambient aerosols

850   with the aerodyne aerosol mass spectrometer, Mass Spectrom. Rev., 26, 185−222,

851   https://doi.org/10.1002/mas.20115, 2007.

852   Canagaratna, M. R., Jimenez, J. L., Kroll, J. H., Chen, Q., Kessler, S. H., Massoli, P.,

853   Hildebrandt Ruiz, L., Fortner, E., Williams, L. R., Wilson, K. R., Surratt, J. D.,

854   Donahue, N. M., Jayne, J. T., and Worsnop, D. R.: Elemental ratio measurements

855   of organic compounds using aerosol mass spectrometry: characterization,

856   improved calibration, and implications, Atmos. Chem. Phys., 15, 253−272,

857   https://doi.org/10.5194/acp-15-253-2015, 2015.

858   Canonaco, F., Crippa, M., Slowik, J. G., Baltensperger, U., and Prévôt, A. S. H.: SoFi,

859   an IGOR-based interface for the efficient use of the generalized multilinear engine

860   (ME-2) for the source apportionment: ME-2 application to aerosol mass

861   spectrometer data, Atmos. Meas. Tech., 6, 3649−3661,

862   https://doi.org/10.5194/amt-6-3649-2013, 2013.

863   Carlton, A. G., Turpin, B. J., Altieri, K. E., Seitzinger, S., Reff, A., Lim, H. J., and

864   Ervens, B.: Atmospheric oxalic acid and SOA production from glyoxal: results of

865   aqueous photooxidation experiments, Atmos. Environ., 41, 7588−7602,

866   https://doi.org/10.1016/j.atmosenv.2007.05.035, 2007.

867   Chen, C. R., Zhang, H. X., Yan, W. J., Wu, N. N., Zhang, Q., and He, K. B.: Aerosol

868   water content enhancement leads to changes in the major formation mechanisms of

869   nitrate and secondary organic aerosols in winter over the North China Plain,

870   Environ. Pollut., 287, 117625, https://doi.org/10.1016/j.envpol.2021.117625, 2021.

871   Chen, Y., Tian, M., Huang, R. J., Shi, G. M., Wang, H. B., Peng, C., Cao, J. J., Wang,

872   Q. Y., Zhang, S. M., Guo, D. M., Zhang, L. Y., and Yang, F. M.: Characterization of

873   urban amine-containing particles in southwestern China: seasonal variation, source,

874   and processing, Atmos. Chem. Phys., 19, 3245−3255,

875   https://doi.org/10.5194/acp-19-3245-2019, 2019.

876   Chen, Y., Xie, S. D., Luo, B., and Zhai, C. Z.: Characteristics and origins of

877   carbonaceous aerosol in the Sichuan Basin, China, Atmos. Environ., 94, 215−223,

878   https://doi.org/10.1016/j.atmosenv.2014.05.037, 2014.

879   Chen, Y., Xie, S. D., Luo, B., and Zhai, C. Z.: Particulate pollution in urban

880   Chongqing of southwest China: Historical trends of variation, chemical

881   characteristics and source apportionment, Sci. Total Environ., 584−585, 523−534,

882   https://doi.org/10.1016/j.scitotenv.2017.01.060, 2017.

883   Coen, M. C., Weingartner, E., Apituley, A., Ceburnis, D., Fierz-Schmidhauser, R.,

884   Flentje, H., Henzing, J. S., Jennings, S. G., Moerman, M., Petzold, A., Schmid, O.,

885   and Baltensperger, U.: Minimizing light absorption measurement artifacts of the

886   Aethalometer: Evaluation of five correction algorithms, Atmos. Meas. Tech., 3,

887   457−474, https://doi.org/10.5194/amt-3-457-2010, 2010.

888   Cubison, M. J., Ortega, A. M., Hayes, P. L., Farmer, D. K., Day, D., Lechner, M. J.,

889   Brune, W. H., Apel, E., Diskin, G. S., Fisher, J. A., Fuelberg, H. E., Hecobian, A.,

890   Knapp, D. J., Mikoviny, T., Riemer, D., Sachse, G. W., Sessions, W., Weber, R. J.,

891   Weinheimer, A. J., Wisthaler, A., and Jimenez, J. L.: Effects of aging on organic

892   aerosol from open biomass burning smoke in aircraft and laboratory studies, Atmos.

893   Chem. Phys., 11, 12049−12064, https://doi.org/10.5194/acp-11-12049-2011, 2011.

894   DeCarlo, P. F., Ulbrich, I. M., Crounse, J., de Foy, B., Dunlea, E. J., Aiken, A. C.,

895   Knapp, D., Weinheimer, A. J., Campos, T., Wennberg, P. O., and Jimenez, J. L.:

896   Investigation of the Sources and Processing of Organic Aerosol over the Central

897   Mexican Plateau from Aircraft Measurements during MILAGRO, Atmos. Chem.

898   Phys., 10, 5257−5280, https://doi.org/10.5194/acp-10-5257-2010, 2010.

899   Drinovec, L., Močnik, G., Zotter, P., Prévôt, A. S. H., Ruckstuhl, C., Coz, E.,

900   Rupakheti, M., Sciare, J., Müller, T., Wiedensohler, A., and Hansen, A. D. A.: The

901   "dual-spot" Aethalometer: an improved measurement of aerosol black carbon with

902   real-time loading compensation, Atmos. Meas. Tech., 8, 1965−1979,

903   https://doi.org/10.5194/amt-8-1965-2015, 2015.

904   Drozd, G. T. and McNeill, V. F.: Organic matrix effects on the formation of

light-absorbing compounds from α-dicarbonyls in aqueous salt solution, Environ. Sci.: Processes Impacts, 16, 741−747, https://doi.org/10.1039/c3em00579h, 2014.

Elser, M., Huang, R. J., Wolf, R., Slowik, J. G., Wang, Q. Y., Canonaco, F., Li, G. H., Bozzetti, C., Daellenbach, K. R., Huang, Y., Zhang, R. J., Li, Z. Q., Cao, J. J., Baltensperger, U., El-Haddad, I., and Prévôt, A. S. H.: New insights into $PM_{2.5}$ chemical composition and sources in two major cities in China during extreme haze events using aerosol mass spectrometry, Atmos. Chem. Phys., 16, 3207−3225, https://doi.org/10.5194/acp-16-3207-2016, 2016.

Ervens, B., Turpin, B. J., and Weber, R. J.: Secondary organic aerosol formation in cloud droplets and aqueous particles (aqSOA): a review of laboratory, field and model studies, Atmos. Chem. Phys., 11, 11069−11102, https://doi.org/10.5194/acp-11-11069-2011, 2011.

Feng, Z., Liu, Y., Zheng, F., Yan, C., Fu, P., Zhang, Y., Lian, C., Wang, W., Cai, J., Du, W., Chu, B., Wang, Y., Kangasluoma, J., Bianchi, F., Petäjä, T., and Kulmala, M.: Highly oxidized organic aerosols in Beijing: Possible contribution of aqueous-phase chemistry, Atmos. Environ., 273, 118971, https://doi.org/10.1016/j.atmosenv.2022.118971, 2022.

Fountoukis, C. and Nenes, A.: ISORROPIA II: a computationally efficient thermodynamic equilibrium model for K^+–Ca^{2+}–Mg^{2+}–NH_4^+–Na^+–SO_4^{2-}–NO_3^-–Cl^-–H_2O aerosols, Atmos. Chem. Phys., 7, 4639−4659, https://doi.org/10.5194/acp-7-4639-2007, 2007.

Fröhlich, R., Cubison, M. J., Slowik, J. G., Bukowiecki, N., Prévôt, A. S. H., Baltensperger, U., Schneider, J., Kimmel, J. R., Gonin, M., Rohner, U., Worsnop, D. R., and Jayne, J. T.: The ToF-ACSM: a portable aerosol chemical speciation monitor with TOFMS detection, Atmos. Meas. Tech., 6, 3225−3241, https://doi.org/10.5194/amt-6-3225-2013, 2013.

Gilardoni, S., Massoli, P., Paglione, M., Giulianelli, L., Carbone, C., Rinaldi, M., Decesari, S., Sandrini, S., Costabile, F., Gobbi, G. P., Pietrogrande, M. C., Visentin, M., Scotto, F., Fuzzi, S., and Facchini, M. C.: Direct observation of aqueous secondary organic aerosol from biomass-burning emissions, Proc. Natl. Acad. Sci.

935   USA, 113, 10013−10018, https://doi.org/10.1073/pnas.1602212113, 2016.

936   Guo, H. Y., Xu, L., Bougiatioti, A., Cerully, K. M., Capps, S. L., Hite Jr., J.R., Carlton,

937   A. G., Lee, S. H., Bergin, M. H., Ng, N. L., Nenes, A., and Weber, R. J.:

938   Fine-particle water and pH in the southeastern United States, Atmos. Chem. Phys.,

939   15, 5211−5228, https://doi.org/10.5194/acp-15-5211-2015, 2015.

940   Gyawali, M., Arnott, W. P., Lewis, K., and Moosmüller, H.: In situ aerosol optics in

941   Reno, NV, USA during and after the summer 2008 California wildfires and the

942   influence of absorbing and non-absorbing organic coatings on spectral light

943   absorption,   Atmos.   Chem.   Phys.,   9,   8007−8015,

944   https://doi.org/10.5194/acp-9-8007-2009, 2009.

945   He, M., Wang, X. R., Han, L., Feng, X. D., and M, X.: Emission Inventory of Crop

946   Residues Field Burning and Its Temporal and Spatial Distribution in Sichuan

947   Province,   Environ.   Sci.,   36,   1208−1216,

948   https://doi.org/10.13227/j.hjkx.2015.04.010, 2015.

949   Hennigan, C. J., Izumi, J., Sullivan, A. P., Weber, R. J., and Nenes, A.: A critical

950   evaluation of proxy methods used to estimate the acidity of atmospheric particles,

951   Atmos. Chem. Phys., 15, 2775–2790, https://doi.org/10.5194/acp-15-2775-2015,

952   2015.

953   Hennigan, C. J., Sullivan, A. P., Collett, J. L., and Robinson, A. L.: Levoglucosan

954   stability in biomass burning particles exposed to hydroxyl radicals, Geophys. Res.

955   Lett., 37, L09806, https://doi.org/10.1029/2010GL043088, 2010.

956   Herrmann, H., Schaefer, T., Tilgner, A., Styler, S. A., Weller, C., Teich, M., and Otto,

957   T.: Tropospheric Aqueous-Phase Chemistry: Kinetics, Mechanisms, and Its

958   Coupling to a Changing Gas Phase, Chem. Rev., 115, 4259−4334,

959   https://doi.org/10.1021/cr500447k, 2015.

960   Huang, R. J., Zhang, Y. L., Bozzetti, C., Ho, K. F., Cao, J. J., Han, Y. M., Daellenbach,

961   K. R., Slowik, J. G., Platt, S. M., Canonaco, F., Zotter, P., Wolf, R., Pieber, S. M.,

962   Bruns, E. A., Crippa, M., Ciarelli, G., Piazzalunga, A., Schwikowski, M.,

963   Abbaszade, G., Schnelle-Kreis, J., Zimmermann, R., An, Z. S., Szidat, S.,

964   Baltensperger, U., El Haddad, I., and Prevot, A. S.: High secondary aerosol

contribution to particulate pollution during haze events in China, Nature, 514, 218−222, https://doi.org/10.1038/nature13774, 2014.

Huang, R. J., He, Y., Duan, J., Li, Y. J., Chen, Q., Zheng, Y., Chen, Y., Hu, W. W., Lin, C. S., Ni, H. Y., Dai, W. T., Cao, J. J., Wu, Y. F., Zhang, R. J., Xu, W., Ovadnevaite, J., Ceburnis, D., Hoffmann, T., and O'Dowd, C. D.: Contrasting sources and processes of particulate species in haze days with low and high relative humidity in wintertime Beijing, Atmos. Chem. Phys., 20, 9101−9114, https://doi.org/10.5194/acp-20-9101-2020, 2020.

Huang, X. J., Liu, Z., Ge, Y. Z., Li, Q., Wang, X. F., Fu, H. B., Zhu, J., Zhou, B., Wang, L., George, C., Wang, Y., Wang, X. F., Su, J. X., Xue, L. K., Yu, S. C., Mellouki, A., and Chen, J. M.: Aerosol high water contents favor sulfate and secondary organic aerosol formation from fossil fuel combustion emissions, npj Clim. Atmos. Sci., 6, 173, https://doi.org/10.1038/s41612-023-00504-1, 2023.

Jimenez, J. L., Canagaratna, M. R., Donahue, N. M., Prevot, A. S. H., Zhang, Q., Kroll, J. H., DeCarlo, P. F., Allan, J. D., Coe, H., Ng, N. L., Aiken, A. C., Docherty, K. S., Ulbrich, I. M., Grieshop, A. P., Robinson, A. L., Duplissy, J., Smith, J. D., Wilson, K. R., Lanz, V. A., Hueglin, C., Sun, Y. L., Tian, J., Laaksonen, A., Raatikainen, T., Rautiainen, J., Vaattovaara, P., Ehn, M., Kulmala, M., Tomlinson, J. M., Collins, D. R., Cubison, M. J., Dunlea, J., Huffman, J. A., Onasch, T. B., Alfarra, M. R., Williams, P. I., Bower, K., Kondo, Y., Schneider, J., Drewnick, F., Borrmann, S., Weimer, S., Demerjian, K., Salcedo, D., Cottrell, L., Griffin, R., Takami, A., Miyoshi, T., Hatakeyama, S., Shimono, A., Sun, J. Y., Zhang, Y. M., Dzepina, K., Kimmel, J. R., Sueper, D., Jayne, J. T., Herndon, S. C., Trimborn, A. M., Williams, L. R., Wood, E. C., Middlebrook, A. M., Kolb, C. E., Baltensperger, U., and Worsnop, D. R.: Evolution of Organic Aerosols in the Atmosphere, Science, 326, 1525−1529, https://doi.org/10.1126/science.1180353, 2009.

Kampf, C. J., Jakob, R., and Hoffmann, T.: Identification and characterization of aging products in the glyoxal/ammonium sulfate system – implications for light-absorbing material in atmospheric aerosols, Atmos. Chem. Phys., 12, 6323−6333, https://doi.org/10.5194/acp-12-6323-2012, 2012.

Kim, H., Collier, S., Ge, X. L., Xu, J. Z., Sun, Y. L., Jiang, W. Q., Wang, Y. L., Herckes, P., and Zhang, Q.: Chemical processing of water-soluble species and formation of secondary organic aerosol in fogs, Atmos. Environ., 200, 158−166, https://doi.org/10.1016/j.atmosenv.2018.11.062, 2019.

Kirchstetter, T. W. and Novakov T.: Evidence that the spectral dependence of light absorption by aerosols is affected by organic carbon, J. Geophys. Res., 109, D21208, https://doi.org/10.1029/2004JD004999, 2004.

Kondo, Y., Komazaki, Y., Miyazaki, Y., Moteki, N., Takegawa, N., Kodama, D., Deguchi, S., Nogami, M., Fukuda, M., Miyakawa, T., Morino, Y., Koike, M., Sakurai, H., and Ehara, K.: Temporal Variations of Elemental Carbon in Tokyo, J. Geophys. Res., 111, D12205, https://doi.org/10.1029/2005JD006257, 2006.

Kourtchev, I., Giorio, C., Manninen, A., Wilson, E., Mahon, B., Aalto, J., Kajos, M., Venables, D., Ruuskanen, T., Levula, J., Loponen, M., Connors, S., Harris, N., Zhao, D. F., Kiendler-Scharr, A., Mentel, T., Rudich, Y., Hallquist, M., Doussin, J. F., Maenhaut, W., Bäck, J., Petäjä, T., Wenger, J., Kulmala, Ma., and Kalberer, M.: Enhanced Volatile Organic Compounds emissions and organic aerosol mass increase the oligomer content of atmospheric aerosols, Sci. Rep., 6, 35038, https://doi.org/10.1038/srep35038, 2016.

Kroflic, A., Grilc, M., and Grgic, I.: Unraveling pathways of guaiacol nitration in atmospheric waters: nitrite, a source of reactive nitronium ion in the atmosphere, Environ. Sci. Technol., 49, 9150−9158, https://doi.org/10.1021/acs.est.5b01811, 2015.

Lack, D. A., and Langridge, J. M.: On the attribution of black and brown carbon light absorption using the Ångström exponent, Atmos. Chem. Phys., 13, 10535−10543, https://doi.org/10.5194/acp-13-10535-2013, 2013.

Lanz, V. A., Alfarra, M. R., Baltensperger, U., Buchmann, B., Hueglin, C., and Prévôt, A. S. H.: Source apportionment of submicron organic aerosols at an urban site by factor analytical modelling of aerosol mass spectra, Atmos. Chem. Phys., 7, 1503−1522, doi:10.5194/acp-7-1503-2007, 2007.

Laskin, A., Laskin, J., and Nizkorodov, S. A.: Chemistry of atmospheric brown carbon,

Chem. Rev., 115, 4335−4382, https://doi.org/10.1021/cr5006167, 2015.

Lee, A. K., Zhao, R., Li, R., Liggio, J., Li, S. M., and Abbatt, J. P.: Formation of Light Absorbing Organo-Nitrogen Species from Evaporation of Droplets Containing Glyoxal and Ammonium Sulfate, Environ. Sci. Technol., 47, 12819−12826, https://doi.org/10.1021/es402687w, 2013.

Lei, Y., Lei, X., Tian, G., Yang, J., Huang, D., Yang, X., Chen, C. C., and Zhao, J. C.: Optical Variation and Molecular Transformation of Brown Carbon During Oxidation by $NO_3\bullet$ in the Aqueous Phase, Environ. Sci. Technol., 58, 3353−3362, https://doi.org/10.1021/acs.est.3c08726, 2024.

Li, C. L., He, Q. F., Fang, Z., Brown, S. S., Laskin, A., Cohen, S. R., and Rudich, Y.: Laboratory Insights into the Diel Cycle of Optical and Chemical Transformations of Biomass Burning Brown Carbon Aerosols, Environ. Sci. Technol., 54, 11827−11837, https://dx.doi.org/10.1021/acs.est.0c04310, 2020.

Li, F. H., Zhou, S. Z., Du, L., Zhao, J., Hang, J., and Wang, X. M.: Aqueous-phase chemistry of atmospheric phenolic compounds: A critical review of laboratory studies, Sci. Total Environ., 856, 158895, https://doi.org/10.1016/j.scitotenv.2022.158895, 2023.

Li, G., Bei, N., Tie, X., and Molina, L. T.: Aerosol effects on the photochemistry in Mexico City during MCMA-2006/MILAGRO campaign, Atmos. Chem. Phys., 11, 5169−5182, https://doi.org/10.5194/acp-11-5169-2011, 2011.

Li, Z. J., Tan, H. B., Zheng, J., Liu, L., Qin, Y. M., Wang, N., Li, F., Li ,Y. J., Cai, M. F., Ma, Y., and Chan, C. K.: Light absorption properties and potential sources of particulate brown carbon in the Pearl River Delta region of China, Atmos. Chem. Phys., 19, 11669−11685, https://doi.org/10.5194/acp-19-11669-2019, 2019.

Lim, Y. B., Tan, Y., Perri, M. J., Seitzinger, S. P., and Turpin, B. J.: Aqueous chemistry and its role in secondary organic aerosol (SOA) formation, Atmos. Chem. Phys., 10, 10521−10539, https://doi.org/10.5194/acp-10-10521-2010, 2010.

Liu, M. X., Song, Y., Zhou, T., Xu, Z. Y., Yan, C. Q., Zheng, M., Wu, Z. J., Hu, M., Wu, Y. S., and Zhu, T.: Fine particle pH during severe haze episodes in northern China, Geophys. Res. Lett., 44, 5213−5221, https://doi.org/10.1002/2017gl073210,

2017.

Liu, Y., Huang, R. J., Lin, C. S., Yuan, W., Li, Y. J., Zhong, H. B., Yang, L., Wang, T., Huang, W., Xu, W., Huang, D. D., and Huang, C.: Nitrate-Photolysis Shortens the Lifetimes of Brown Carbon Tracers from Biomass Burning, Environ. Sci. Technol., 59, 640−649, https://doi.org/10.1021/acs.est.4c06123, 2024.

Lorenzo, R. A. D., Washenfelder, R. A., Attwood, A. R., Guo, H., Xu, L., Ng, N. L., Weber, R. J., Baumann, K., Edgerton, E., and Young, C. J.: Molecular-Size-Separated Brown Carbon Absorption for Biomass-Burning Aerosol at Multiple Field Sites, Environ. Sci. Technol., 51, 3128−3137, https://doi.org/10.1021/acs.est.6b06160, 2017.

Lu, Z., Streets, D. G., Winijkul, E., Yan, F., Chen, Y., Bond, T. C., Feng, Y., Dubey, M. K., Liu, S., Pinto, J. P., and Carmichael, G. R.: Light absorption properties and radiative effects of primary organic aerosol emissions, Environ. Sci. Technol., 49, 4868−4877, https://doi.org/10.1021/acs.est.5b00211, 2015.

Luo, J. Q., Zhang, J. K., Huang, X. J ., Liu, Q., Luo, B., Zhang, W., Rao, Z. H., and Yu, Y. C.: Characteristics, evolution, and regional differences of biomass burning particles in the Sichuan Basin, China, J. Environ. Sci., 89, 35−46, https://doi.org/10.1016/j.jes.2019.09.015, 2020.

Matthew, B. M., Middlebrook, A. M., and Onasch, T. B.: Collection Efficiencies in an Aerodyne Aerosol Mass Spectrometer as a Function of Particle Phase for Laboratory Generated Aerosols, Aerosol Sci. Technol., 42, 884−898, https://doi.org/10.1080/02786820802356797, 2008.

McNeill, V. F.: Aqueous Organic Chemistry in the Atmosphere: Sources and Chemical Processing of Organic Aerosols, Environ. Sci. Technol., 49, 1237−1244, https://doi.org/10.1021/es5043707, 2015.

Meng, J. J., Liu, X. D., Hou, Z. F., Yi, Y. A., Yan, L., Li, Z., Cao, J. J., Li, J. J., and Wang, G. H.: Molecular characteristics and stable carbon isotope compositions of dicarboxylic acids and related compounds in the urban atmosphere of the North China Plain: Implications for aqueous phase formation of SOA during the haze periods, Sci. Total Environ., 705, 135256,

1085   https://doi.org/10.1016/j.scitotenv.2019.135256, 2020.

1086   Middlebrook, A. M., Bahreini, R., Jimenez, J. L., and Canagaratna, M. R.: Evaluation

1087   of Composition-Dependent Collection Efficiencies for the Aerodyne Aerosol Mass

1088   Spectrometer using Field Data, Aerosol Sci. Technol., 46, 258−271,

1089   https://doi.org/10.1080/02786826.2011.620041, 2012.

1090   Ministry of Environmental Protection (MEP): P.R. Of China, China National Ambient

1091   Air Quality Standard (GB 3095-2012), http://kjs.mep.

1092   gov.cn/hjbhbz/bzwb/dqhjbh/dqhjzlbz/201203/t20120302_224165.htm, 2012.

1093   Moosmüller, H., Chakrabarty, R. K., and Arnott, W. P.: Aerosol light absorption and

1094   its measurement: A review, J. Quant. Spectrosc. Ra., 110, 844−878,

1095   https://doi.org/10.1016/j.jqsrt.2009.02.035, 2009.

1096   Ng, N. L., Canagaratna, M. R., Jimenez, J. L., Chhabra, P. S., Seinfeld, J. H., and

1097   Worsnop, D. R.: Changes in organic aerosol composition with aging inferred from

1098   aerosol mass spectra, Atmos. Chem. Phys., 11, 6465−6474,

1099   https://doi.org/10.5194/acp-11-6465-2011, 2011a.

1100   Ng, N. L., Canagaratna, M. R., Jimenez, J. L., Zhang, Q., Ulbrich, I. M., and Worsnop,

1101   D. R.: Real-Time Methods for Estimating Organic Component Mass

1102   Concentrations from Aerosol Mass Spectrometer Data, Environ. Sci. Technol., 45,

1103   910−916, https://doi.org/10.1021/es102951k, 2011b.

1104   Ng, N. L., Canagaratna, M. R., Zhang, Q., Jimenez, J. L., Tian, J., Ulbrich, I. M.,

1105   Kroll, J. H., Docherty, K. S., Chhabra, P. S., Bahreini, R., Murphy, S. M., Seinfeld,

1106   J. H., Hildebrandt, L., Donahue, N. M., DeCarlo, P. F., Lanz, V. A., Prévôt, A. S. H.,

1107   Dinar, E., Rudich, Y., and Worsnop, D. R.: Organic aerosol components observed

1108   in Northern Hemispheric datasets from Aerosol Mass Spectrometry, Atmos. Chem.

1109   Phys., 10, 4625−4641, https://doi.org/10.5194/acp-10-4625-2010, 2010.

1110   Ng, N. L., Herndon, S. C., Trimborn, A., Canagaratna, M. R., Croteau, P. L., Onasch,

1111   T. B., Sueper, D., Worsnop, D. R., Zhang, Q., Sun, Y. L., and Jayne J. T.: An

1112   Aerosol Chemical Speciation Monitor (ACSM) for Routine Monitoring of the

1113   Composition and Mass Concentrations of Ambient Aerosol, Aerosol Sci. Technol.,

1114   45, 780−794, https://doi.org/10.1080/02786826.2011.560211, 2011c.

Nguyen, T. K. V., Zhang, Q., Jimenez, J. L., Pike, M., and Carlton, A. G.: Liquid Water: Ubiquitous Contributor to Aerosol Mass, Environ. Sci. Technol. Lett., 3, 257−263, https://doi.org/10.1021/acs.estlett.6b00167, 2016.

Nozière, B., and Esteve, W.: Light-absorbing aldol condensation products in acidic aerosols: Spectra, kinetics, and contribution to the absorption index, Atmos. Environ., 41, 1150−1163, https://doi.org/10.1016/j.atmosenv.2006.10.001, 2007.

Nozière, B., Dziedzic, P., and Córdova, A.: Products and Kinetics of the Liquid-Phase Reaction of Glyoxal Catalyzed by Ammonium Ions (NH_4^+), J. Phys. Chem. A, 113, 231−237, https://doi.org/10.1021/jp8078293, 2009.

Ortega, A. M., Ortega, D. A., Cubison, M. J., Brune, W. H., Bon, D., Gouw de, J. A., and Jimenez, J. L.: Secondary organic aerosol formation and primary organic aerosol oxidation from biomass-burning smoke in a flow reactor during FLAME-3, Atmos. Chem. Phys., 13, 11551−11571, https://doi.org/10.5194/acp-13-11551-2013, 2013.

Ortiz-Montalvo, D. L., Lim, Y. B., Perri, M. J., Seitzinger, S. P., and Turpin, B. J.: Volatility and Yield of Glycolaldehyde SOA Formed through Aqueous Photochemistry and Droplet Evaporation, Aerosol Sci. Technol., 46, 1002−1014, https://doi.org/10.1080/02786826.2012.686676, 2012.

Paatero, P.: The Multilinear Engine: A Table-Driven, Least Squares Program for Solving Multilinear Problems, Including the n-Way Parallel Factor Analysis Model, J. Comput. Graph. Stat., 8, 854−888, https://doi.org/10.1080/10618600.1999.10474853, 1999.

Paatero, P. and Hopke, P. K.: Discarding or downweighting high-noise variables in factor analytic models, Anal. Chim. Acta., 490, 277−289, https://doi.org/10.1016/S0003-2670(02)01643-4, 2003.

Paatero, P. and Tapper, U.: Positive matrix factorization: A non-negative factor model with optimal utilization of error estimates of data values, Environmetrics, 5, 111−126, https://doi.org/10.1002/env.3170050203, 1994.

Paglione, M., Gilardoni, S., Rinaldi, M., Decesari, S., Zanca, N., Sandrini, S., Giulianelli, L., Bacco, D., Ferrari, S., Poluzzi, V., Scotto, F., Trentini, A., Poulain,

L., Herrmann, H., Wiedensohler, A., Canonaco, F., Prévôt, A. S. H., Massoli, P., Carbone, C., Facchini, M. C., and Fuzzi, S. C.: The impact of biomass burning and aqueous-phase processing on air quality: a multi-year source apportionment study in the Po Valley, Italy, Atmos. Chem. Phys., 20, 1233−1254, https://doi.org/10.5194/acp-20-1233-2020, 2020.

Pang, H. W., Zhang, Q., Lu, X. H., Li, K. N., Chen, H., Chen, J. M., Yang, X., Ma, Y. G., Ma, J. L., and Huang, C.: Nitrite-Mediated Photooxidation of Vanillin in the Atmospheric Aqueous Phase, Environ. Sci. Technol., 53, 14253−14263, https://doi.org/10.1021/acs.est.9b03649, 2019.

Peng, C., Tian, M., Chen, Y., Wang, H. B., Zhang, L. M., Shi, G. M., Liu, Y., Yang, F. M., and Zhai, C. Z.: Characteristics, Formation Mechanisms and Potential Transport Pathways of $PM_{2.5}$ at a Rural Background Site in Chongqing, Southwest China, Aerosol Air Qual. Res., 19, 1980−1992, https://doi.org/10.4209/aaqr.2019.01.0010, 2019.

Peng, C., Tian, M., Shi, G. M., Zhang, S. M., Long, X., Che, H. X., Zhong, J., You, X. Y., Bao, Z. E., Yang, F. M., Qi, X., Zhai, C. Z., and Chen, Y.: Sources and light absorption of brown carbon in urban areas of the Sichuan Basin, China: Contribution from biomass burning and secondary formation, Atmos. Res., 318, 107992, https://doi.org/10.1016/j.atmosres.2025.107992, 2025.

Powelson, M. H., Espelien, B. M., Hawkins, L. N., Galloway, M. M., and Haan, D. O. D.: Brown Carbon Formation by Aqueous-Phase Carbonyl Compound Reactions with Amines and Ammonium Sulfate, Environ. Sci. Technol., 48, 985−993, https://doi.org/10.1021/es4038325, 2014.

Qin, Y. M., Tan, H. B., Li, Y. J., Li, Z. J., Schurman, M. I., Liu, L., Wu, C., and Chan, C. K.: Chemical characteristics of brown carbon in atmospheric particles at a suburban site near Guangzhou, China, Atmos. Chem. Phys., 18, 16409−16418, https://doi.org/10.5194/acp-18-16409-2018, 2018.

Qiu, X., Duan, L., Chai, F., Wang, S., Yu, Q., and Wang, S.: Deriving High-Resolution Emission Inventory of Open Biomass Burning in China based on Satellite Observations, Environ. Sci. Technol., 50, 11779−11786,

https://doi.org/10.1021/acs.est.6b02705, 2016.

Saleh, R., Hennigan, C. J., McMeeking, G. R., Chuang, W. K., Robinson, E. S., Coe, H., Donahue, N. M., and Robinson, A. L.: Absorptivity of brown carbon in fresh and photo-chemically aged biomass-burning emissions, Atmos. Chem. Phys., 13, 7683−7693, https://doi.org/10.5194/acp-13-7683-2013, 2013.

Saleh, R., Robinson, E. S., Tkacik, D. S., Ahern, A. T., Liu, S., Aiken, A. C., Sullivan, R. C., Presto, A. A., Dubey, M. K., Yokelson, R. J., Donahue, N. M., and Robinson, A. L.: Brownness of organics in aerosols from biomass burning linked to their black carbon content, Nat. Geosci., 7, 647−650, https://doi.org/10.1038/ngeo2220, 2014.

Sareen, N., Moussa, S. G., and McNeill, V. F.: Photochemical Aging of Light-Absorbing Secondary Organic Aerosol Material, J. Phys. Chem. A, 117, 2987−2996, https://doi.org/10.1021/jp309413j, 2013.

Shrivastava, M., Cappa, C. D., Fan, J. W., Goldstein, A. H., Guenther, A. B., Jimenez, J. L., Kuang, C. A., Laskin, A., Martin, S. T., Ng, N. L., Petaja, T., Pierce, J. R., Rasch, P. J., Roldin, P., Seinfeld, J. H., Shilling, J., Smith, J. N., Thornton, J. A., Volkamer, R., Wang, J., Worsnop, D. R., Zaveri, R. A., Zelenyuk, A., and Zhang, Q.: Recent advances in understanding secondary organic aerosol: Implications for global climate forcing, Rev. Geophys., 55, 509−559, doi:10.1002/2016RG000540, 2017.

Sun, Y. L., Du, W., Fu, P. Q., Wang, Q. Q., Li, J., Ge, X. L., Zhang, Q., Zhu, C. M., Ren, L. J., Xu, W. Q., Zhao, J., Han, T. T., Worsnop, D. R., and Wang, Z. F.: Primary and secondary aerosols in Beijing in winter: sources, variations and processes, Atmos. Chem. Phys., 16, 8309−8329, https://doi.org/10.5194/acp-16-8309-2016, 2016a.

Sun, Y. L., Jiang, Q., Xu, Y. S., Ma, Y., Zhang, Y. J., Liu, X. G., Li, W. J., Wang, F., Li, J., Wang, P. C., and Li, Z. Q.: Aerosol characterization over the North China Plain: Haze life cycle and biomass burning impacts in summer, J. Geophys. Res.: Atmos., 121, 2508−2521, https://doi.org/10.1002/ 2015jd024261, 2016b.

Sun, Y. L., Zhang, Q., Anastasio, C., and Sun, J.: Insights into secondary organic

aerosol formed via aqueous-phase reactions of phenolic compounds based on high resolution mass spectrometry, Atmos. Chem. Phys., 10, 4809−4822, https://doi.org/10.5194/acp-10-4809-2010, 2010.

Tan, Y., Lim, Y. B., Altieri, K. E., Seitzinger, S. P., and Turpin, B. J.: Mechanisms leading to oligomers and SOA through aqueous photooxidation: insights from OH radical oxidation of acetic acid and methylglyoxal, Atmos. Chem. Phys., 12, 801−813, https://doi.org/10.5194/acp-12-801-2012, 2012.

Tang, H. H., Li, Z. L., Tian, M., Peng, C., Ding, Y., Chen, M. L., Wang, X., C., Chen, Y., Yang, F. M., and Zhai, C. Z.: Formation of Oxidized Organic Aerosols in Winter Haze in a Megacity of Southwest China: Implication for the Importance of Biomass Burning, J. Geophys. Res. Atmos., 130, e2025JD044028, https://doi.org/10.1029/2025JD044028, 2025.

Tao, J., Gao, J., Zhang, L., Zhang, R., Che, H., Zhang, Z., Lin, Z., Jing, J., Cao, J., and Hsu, S. C.: $PM_{2.5}$ pollution in a megacity of southwest China: source apportionment and implication, Atmos. Chem. Phys., c14, 8679−8699, https://doi.org/10.5194/acp-14-8679-2014, 2014.

Tian M., Liu Y., Yang F. M., Zhang L. M., Peng C., Chen Y., Shi G. M., Wang H. B., Luo B., Jiang C. T., Li B., Takeda N., and Koizumi K.: Increasing importance of nitrate formation for heavy aerosol pollution in two megacities in Sichuan Basin, southwest China, Environ. Pollut., 250, 898−905, https://doi.org/10.1016/j.envpol.2019.04.098, 2019.

Wang, G. H., Zhang, R. Y., Gomez, M. E., Yang, L. X., Zamora, M. L., Hu, M., Lin, Y., Peng, J. F., Guo, S., Meng, J. J., Li, J. J., Cheng, C. L., Hu T. F., Ren, Y. Q., Wang, Y. S., Gao, J., Cao, J. J., An, Z. S., Zhou, W. J., Li, G. H., Wang, J. Y., Tian, P. F., Marrero-Ortiz, W., Secrest, J., Du, Z. F., Zheng, J., Shang, D. J., Zeng, L. M., Shao, M., Wang, W. G., Huang, Y., Wang, Y., Zhu, Y. J., Li, Y. X., Hu, J. X., Pan, B., Cai, L., Cheng, Y. T., Ji, Y. M., Zhang, F., Rosenfeld, D., Liss, P. S., Duce, R. A., Kolb, C. E., and Molina, M. J.: Persistent sulfate formation from London Fog to Chinese haze, Proc. Natl. Acad. Sci. USA, 113, 13630−13635, https://doi.org/10.1073/pnas.1616540113, 2016.

Wang, H. B., Tian, M., Chen, Y., Shi, G. M., Liu, Y., Yang, F. M., Zhang, L. M., Deng, L. Q., Yu, J. Y., Peng, C., and Cao, X. Y.: Seasonal characteristics, formation mechanisms and source origins of $PM_{2.5}$ in two megacities in Sichuan Basin, China, Atmos. Chem. Phys., 18, 865−881, https://doi.org/10.5194/acp-18-865-2018, 2018.

Wang, H. B., Zhang, L. M., Huo, T. T., Wang, B., Yang, F. M., Chen, Y., Tian, M., Qiao, B. Q., and Peng, C.: Application of parallel factor analysis model to decompose excitation-emission matrix fluorescence spectra for characterizing sources of water-soluble brown carbon in $PM_{2.5}$, Atmos. Environ., 223, 117192, https://doi.org/10.1016/j.atmosenv.2019.117192, 2019a.

Wang, J. F., Ye, J. H., Zhang, Q., Zhao, J., Wu, Y. Z., Li, J. Y., Liu, D. T., Li, W. J., Zhang, Y. G., Wu, C., Xie, C. H., Qin, Y. M., Lei, Y. L., Huang, X. P., Guo, J. P., Liu, P. F., Fu, P. Q., Li, Y. J., Lee, H. C., Choi, H., Zhang, J., Liao, H., Chen, M. D., Sun, Y. L., Ge, X. L., Martin, S. T., and Jacob, D. J.: Aqueous production of secondary organic aerosol from fossil-fuel emissions in winter Beijing haze, Proc. Natl. Acad. Sci. USA, 118, e2022179118, https://doi.org/10.1073/pnas.2022179118, 2021.

Wang, Q. Y., Ye, J. H., Wang, Y. C., Zhang, T., Ran, W. K., Wu, Y. F., Tian, J., Li, L., Zhou, Y. Q., Ho, H. S. S., Dang, B., Zhang, Q., Zhang, R. J., Chen, Y., Zhu, C. S., and Cao, J. J.: Wintertime Optical Properties of Primary and Secondary Brown Carbon at a Regional Site in the North China Plain, Environ. Sci. Technol., 53, 12389−12397, https://doi.org/10.1021/acs.est.9b03406, 2019b.

Washenfelder, R. A., Attwood, A. R., Brock, C. A., Guo, H., Xu, L., Weber, R. J., Ng, N. L., Allen, H. M., Ayres, B. R., Baumann, K., Cohen, R. C., Draper, D. C., Duffey, K. C., Edgerton, E., Fry, J. L., Hu, W. W., Jimenez, J. L., Palm, B. B., Romer, P., Stone, E. A., Wooldridge, P. J., and Brown, S. S.: Biomass burning dominates brown carbon absorption in the rural southeastern United States, Geophys. Res. Lett., 42, 653−664, https://doi.org/10.1002/2014gl062444, 2015.

Wu, C. and Yu, J. Z.: Determination of primary combustion source organic carbon-to-elemental carbon (OC/EC) ratio using ambient OC and EC measurements: Secondary OC-EC correlation minimization method, Atmos. Chem.

Phys., 16, 5453−5465, https://doi.org/10.5194/acp-16-5453-2016, 2016.

Wu, H., Peng, C., Zhai, T. Y., Deng, J. C., Lu, P. L., Li, Z. L., Chen, Y., Tian, M., Bao, Z. E., Long, X., Yang, F. M., and Zhai, C. Z.: Characteristics of light absorption and environmental effects of Brown carbon aerosol in Chongqing during summer and winter based on online measurement: Implications of secondary formation, Atmos. Environ., 338, 120843, https://doi.org/10.1016/j.atmosenv.2024.120843, 2024.

Xie, C. H., Xu, W. Q., Wang, J. F., Wang, Q. Q., Liu, D. T., Tang, G. Q., Chen, P., Du, W., Zhao, J., Zhang, Y. J., Zhou, W., Han, T. T., Bian, Q. Y., Li, J., Fu, P. Q., Wang, Z. F., Ge, X. L., Allan, J., Coe, H., and Sun, Y. L.: Vertical characterization of aerosol optical properties and brown carbon in winter in urban Beijing, China, Atmos. Chem. Phys., 19, 165−179, https://doi.org/10.5194/acp-19-165-2019, 2019.

Xu, B. Q., Zhang, G., Gustafsson, Ö., Kawamura, K., Li, J., Andersson, A., Bikkina, S., Kunwar, B., Pokhrel, A., Zhong, G. C., Zhao, S. Z., Li, J., Huang, C., Cheng, Z. N., Zhu, S. Y., Peng, P. A., and Sheng, G. Y.: Large contribution of fossil-derived components to aqueous secondary organic aerosols in China, Nat. Commun., 13, 5115, https://doi.org/10.1038/s41467-022-32863-3, 2022.

Xu, W. Q., Han, T. T., Du, W., Wang, Q. Q., Chen, C., Zhao, J., Zhang, Y. J., Li, J., Fu, P. Q., Wang, Z. F., Worsnop, D. R., and Sun, Y. L.: Effects of Aqueous-Phase and Photochemical Processing on Secondary Organic Aerosol Formation and Evolution in Beijing, China, Environ. Sci. Technol., 51, 762−770, https://doi.org/10.1021/acs.est.6b04498, 2017.

Xu, W. Q., Sun, Y. L., Chen, C., Du, W., Han, T. T., Wang, Q. Q., Fu, P. Q., Wang, Z. F., Zhao, X. J., Zhou, L. B., Ji, D. S., Wang, P. C., and Worsnop, D. R.: Aerosol composition, oxidation properties, and sources in Beijing: results from the 2014 Asia-Pacific Economic Cooperation summit study, Atmos. Chem. Phys., 15, 13681−13698, https://doi.org/10.5194/acp-15-13681-2015, 2015.

Xu, W. Q., Sun, Y. L., Wang, Q. Q., Zhao, J., Wang, J. F., Ge, X. L., Xie, C. J., Zhou, W., Du, W., Li, J., Fu, P. Q., Wang, Z. F., Worsnop, D. R., and Coe, H.: Changes in Aerosol Chemistry From 2014 to 2016 in Winter in Beijing: Insights From

High-Resolution Aerosol Mass Spectrometry, J. Geophys. Res.: Atmos., 124, 1132−1147, https://doi.org/10.1029/2018JD029245, 2019.

Yan, C. Q., Zheng, M., Bosch, C., Andersson, A., Desyaterik, Y., Sullivan, A. P., Collett, J. L., Zhao, B., Wang, S. X., He, K. B., and Gustafsson, Ö.: Important fossil source contribution to brown carbon in Beijing during winter, Sci. Rep., 7, 43182, https://doi.org/10.1038/srep43182, 2017.

Yang, F. M., Tan, J., Zhao, Q., Du, Z., He, K. B., Ma, Y. L., Duan, F. K., Chen, G., and Zhao, Q.: Characteristics of $PM_{2.5}$ speciation in representative megacities and across China, Atmos. Chem. Phys., 11, 5207−5219, https://doi.org/10.5194/acp-11-5207-2011, 2011.

Yang, J. W., Au, W. C., Law, H., Lam, C. H., and Nah, T.: Formation and evolution of brown carbon during aqueous-phase nitrate-mediated photooxidation of guaiacol and 5-nitroguaiacol, Atmos. Environ., 254, 118401, https://doi.org/10.1016/j.atmosenv.2021.118401, 2021.

Yang, W., Xie, S., Zhang, Z., Hu, J., Zhang, L., Lei, X., Zhong, L., Hao, Y., and Shi, F.: Characteristics and sources of carbonaceous aerosol across urban and rural sites in a rapidly urbanized but low-level industrialized city in the Sichuan Basin, China, Environ. Sci. Pollut. R., 26, 26646−26663, https://doi.org/10.1007/s11356-019-05242-7, 2019.

Ye, Z. L., Qu, Z. X., Ma, S. S., Luo, S. P., Chen, Y. T., Chen, H., Chen, Y. F., Zhao, Z. Z., Chen, M. D., and Ge, X. L.: A comprehensive investigation of aqueous-phase photochemical oxidation of 4-ethylphenol, Sci. Total Environ., 685, 976−985, https://doi.org/10.1016/j.scitotenv.2019.06.276, 2019.

Yokelson, R. J., Urbanski, S. P., Atlas, E. L., Toohey, D. W., Alvarado, E. C., Crounse, J. D., Wennberg, P. O., Fisher, M. E., Wold, C. E., Campos, T. L., Adachi, K., Buseck, P. R., and Hao, W. M.: Emissions from forest fires near Mexico City, Atmos. Chem. Phys., 7, 5569−5584, https://doi.org/10.5194/acp-7-5569-2007, 2007.

Yu, L., Smith, J., Laskin, A., Anastasio, C., Laskin, J., Zhang, Q.: Chemical characterization of SOA formed from aqueous-phase reactions of phenols with the

triplet excited state of carbonyl and hydroxyl radical, Atmos. Chem. Phys., 14, 13801−13816, https://doi.org/10.5194/acp-14-13801-2014, 2014.

Yu, L., Smith, J., Laskin, A., George, K. M., Anastasio, C., Laskin, J., Dillner, A. M., and Zhang, Q.: Molecular transformations of phenolic SOA during photochemical aging in the aqueous phase: competition among oligomerization, functionalization, and fragmentation, Atmos. Chem. Phys., 16, 4511−4527, https://doi.org/10.5194/acp-16-4511-2016, 2016.

Zeng, X., Bao, Z., Zhou, J., Shi, G., Zhou, L., Zhang, S., Qi, X., Lu, K., Zhai, C., Li, Z., Li, X., Peng, C., Yang, F., Tang, M., Feng, M., Tan, Q., and Chen, Y.: Effects of photochemical and aqueous-phase oxidation on secondary formation during the 31st FISU Summer World University Games, 2023, J. Environ. Sci., 162, 810−820, https://doi.org/10.1016/j.jes.2025.08.039, 2025.

Zhang, X. Y., Bao, Z. R., Zhang, L. Y., Zhou, J. W., Che, H. X., Li, Q., Tian, M., Yang, F. M., and Chen, Y.: Biomass burning and aqueous reactions drive the elevation of wintertime $PM_{2.5}$ in the rural area of the Sichuan basin, China, Atmos. Environ., 306, 119779, https://doi.org/10.1016/j.atmosenv.2023.119779, 2023.

Zhang, X. Y., Liu, H. X., Cheng, J. L., Song, W., Wang, H. C., Zhang, Y. L., and Wang, X. M.: Gas-Phase Oxidation of Guaiacol by NO_3 Radicals: Kinetic Measurements and Implications, ACS ES&T Air, 2, 903−910, https://doi.org/10.1021/acsestair.4c00353, 2025.

Zhao, J., Du, W., Zhang, Y. J., Wang, Q. Q., Chen, C., Xu, W. Q., Han, T. T., Wang, Y. Y., Fu, P. Q., Wang, Z. F., Li, Z. Q., and Sun, Y. L.: Insights into aerosol chemistry during the 2015 China Victory Day parade: results from simultaneous measurements at ground level and 260 m in Beijing, Atmos. Chem. Phys., 17, 3215−3232, https://doi.org/10.5194/acp-17-3215-2017, 2017.

Zhao, J., Qiu, Y. M.,Zhou, W., Xu, W. Q., Wang, J. F., Zhang, Y. J., Li, L. J., Xie, C. H., Wang, Q. Q., Du, W., Worsnop, D. R., Canagaratna, M. R., Zhou, L. B., Ge, X. L., Fu, P. Q., Li, J., Wang, Z. F., Donahue, N. M., and Sun, Y. L.: Organic Aerosol Processing During Winter Severe Haze Episodes in Beijing, J. Geophys. Res.: Atmos., 124, 10248−10263, https://doi.org/10.1029/2019JD030832, 2019.

1355 Zhao, R., Lee, A. K. Y., Huang, L., Li, X., Yang, F., and Abbatt, J. P. D.:
1356   Photochemical processing of aqueous atmospheric brown carbon, Atmos. Chem.
1357   Phys., 15, 6087−6100, https://doi.org/10.5194/acp-15-6087-2015, 2015.

1358 Zhao, R., Mungall, E. L., Lee, A. K. Y., Aljawhary, D., and Abbatt, J. P. D.:
1359   Aqueous-phase photooxidation of levoglucosan – a mechanistic study using
1360   aerosol time-of-flight chemical ionization mass spectrometry (Aerosol ToF-CIMS),
1361   Atmos. Chem. Phys., 14, 9695−9706, https://doi.org/10.5194/acp-14-9695-2014,
1362   2014.

1363 Zhong, H. B., Huang, R. J., Chang, Y. H., Duan, J., Lin, C. S., and Chen, Y.:
1364   Enhanced formation of secondary organic aerosol from photochemical oxidation
1365   during the COVID-19 lockdown in a background site in Northwest China, Sci.
1366   Total Environ., 778, 144947, https://doi.org/10.1016/j.scitotenv.2021.144947,
1367   2021.

1368 Zhu, C. S., Cao, J. J., Hu, T. F., Shen, Z. X., Tie, X. X., Huang, H., Wang, Q. Y.,
1369   Huang, R. J., Zhao, Z. Z., Mocnik, G., and Hansen, A. D. A.: Spectral dependence
1370   of aerosol light absorption at an urban and a remote site over the Tibetan Plateau,
1371   Sci. Total Environ., 590−591, 14−21,
1372   https://doi.org/10.1016/j.scitotenv.2017.03.057, 2017.

1373 Zhu, L. W., Cui, Y. J., Ge, X. L., Ye, Z. l., and Zhao, Z. Z.: Aqueous-phase
1374   photochemical oxidation of extracted WSOC in $PM_{2.5}$ from biomass burning,
1375   China Environ. Sci., 43, 1014−1025,
1376   https://doi.org/10.19674/j.cnki.issn1000-6923.20220928.004, 2023.